



HAL
open science

Zn-Al layered double hydroxide-based nanocomposite functionalized with an octahedral molybdenum cluster exhibiting prominent photoactive and oxidation properties

T.K.N. Nguyen, L.Y. Matsui, Naoto Shirahata, N. Dumait, Stéphane Cordier, Fabien Grasset, N. Ohashi, Tetsuo Uchikoshi

► To cite this version:

T.K.N. Nguyen, L.Y. Matsui, Naoto Shirahata, N. Dumait, Stéphane Cordier, et al.. Zn-Al layered double hydroxide-based nanocomposite functionalized with an octahedral molybdenum cluster exhibiting prominent photoactive and oxidation properties. *Applied Clay Science*, 2020, 196, pp.105765. 10.1016/j.clay.2020.105765 . hal-02931981

HAL Id: hal-02931981

<https://hal.science/hal-02931981>

Submitted on 9 Sep 2020

HAL is a multi-disciplinary open access archive for the deposit and dissemination of scientific research documents, whether they are published or not. The documents may come from teaching and research institutions in France or abroad, or from public or private research centers.

L'archive ouverte pluridisciplinaire **HAL**, est destinée au dépôt et à la diffusion de documents scientifiques de niveau recherche, publiés ou non, émanant des établissements d'enseignement et de recherche français ou étrangers, des laboratoires publics ou privés.

Zn-Al layered double hydroxide-based nanocomposite functionalized with an octahedral molybdenum cluster exhibiting prominent photoactive and oxidation properties

Ngan Thi Kim Nguyen^{1,2}, Yoshio Matsui¹, Naoto Shirahata³, Noée Dumait⁴, Stéphane Cordier⁴, Fabien Grasset^{1,2,4}, Naoki Ohashi^{1,2} and Tetsuo Uchikoshi^{1,2*}

1) Research Center for Functional Materials, National Institute for Materials Science (NIMS), 1-2-1 Sengen, Tsukuba, Ibaraki 305-0047, Japan

2) CNRS–Saint-Gobain–NIMS, UMI 3629, Laboratory for Innovative Key Materials and Structures (LINK), National Institute for Materials Science, 1-1 Namiki, Tsukuba, Ibaraki 305-0044, Japan

3) Research Center for Materials Nanoarchitectonics (MANA), National Institute for Materials Science (NIMS), 1-1 Namiki, Tsukuba 305-0044, and Japan

4) Univ. Rennes, ENSCR, INSA Rennes, CNRS, ISCR (Institut des Sciences Chimiques de Rennes) – UMR 6226, F-35000 Rennes, France

Corresponding author:

Tetsuo UCHIKOSHI

Full postal address: Research Center for Functional Materials, National Institute for Materials Science (NIMS), 1-2-1 Sengen, Tsukuba, Ibaraki 305-0047, Japan

Telephone: +81-29-859-2460 / Fax: +81-29-859-2401

E-Mail address: UCHIKOSHI.Tetsuo@nims.go.jp

24

25 Thi Kim Ngan NGUYEN

26 Full postal address: Research Center for Functional Materials, National Institute for
27 Materials Science (NIMS), 1-2-1 Sengen, Tsukuba, Ibaraki 305-0047, Japan

28 E-Mail address: NGUYEN.Thikimngan@nims.go.jp

29

30 **Abstract**

31 A new layered double hydroxide (LDH)-based nanocomposite functionalized with an
32 octahedral molybdenum atom cluster (MC) exhibiting prominent photoactive and
33 oxidation properties was synthesized. Zn-Al LDH and Zn-Al LDH intercalated dodecyl
34 sulfate compounds (abbreviated as LDH-1 and LDH-2 respectively) were prepared by
35 the co-precipitation method in an aqueous solution. The MCs were simply introduced
36 into the LDH-2 by an anion exchangeable method in dimethylformamide under ambient
37 conditions. The extension of the basal spacing of the LDH-1 from 0.9 nm to about 5 nm
38 by intercalating dodecyl sulfate and Mo₆ cluster was confirmed by several
39 complementary technics. The octahedral structure of the Mo₆ cluster was retained after
40 the modification process in an organic dispersing medium that was confirmed by
41 ultraviolet-visible absorption and photoluminescence experiments. The possible
42 chemical bonding between the $[\text{Mo}_6\text{Cl}_8\text{Cl}_{6-x-y}(\text{H}_2\text{O})_x(\text{OH})_y]^{x-2}$ ($x = 0, 1$ or 2 and $y = 0,$
43 $1, 2, 3$; $x + y = 3$) clusters and LDH-2 was suggested on the basis of by X-ray
44 photoelectron spectroscopy. The excellent photoactive and oxidation performance of the
45 Mo₆ cluster on the methylene blue degradation in an aqueous solution was determined
46 in the dark, under UV light ($\lambda = 370$ nm) or with the existence of H₂O₂. The combination
47 of the LDH-2 with a high absorbability and recyclability and the Mo₆ cluster will be a

48 promising candidate as a heterogenized homogeneous catalyst for removing organic
49 pollutants.

50 **KEYWORDS:** molybdenum, octahedral cluster, outer surface functionalization, layered
51 double hydroxide, photochemistry, pollutant degradation

52

53 **1. INTRODUCTION**

54 Among the various wastewater treatment techniques, the adsorption has been proposed
55 as one of the best methods due to its inexpensiveness, universal nature, and ease of
56 operation. Many studies have paid attention to determining new functional and large-
57 scale productive materials for removing organic pollutants by adsorption combined with
58 photocatalytic degradation [1]. This approach becomes an important pathway for
59 pharmaceutical contaminant removal that attracts huge interests of the studies based on
60 TiO₂, ZnO, or graphene-functionalized materials [2, 3]. Besides, layered double
61 hydroxides (LDH) are well known as important compounds due to their interlayer anion
62 exchangeability and potential material for industrial-scale applications such that their
63 fundamental understanding in heterogeneous catalysis, water treatment, and drug
64 delivery is developed [4-5]. LDH with the general formula of $[M^{2+}_x M^{3+}_x(OH)_2]^{x+}[A^{n-}]_{x/n} \cdot mH_2O$ (x as the molar ratio $M^{2+}/(M^{2+} + M^{3+})$ in the range 0.2–
65 0.33) is composed of the divalent and trivalent metals occupying at the octahedral center
66 [6]. The positive charges on the metal hydroxide layers are generated by the exchange
67 of the divalent metals (Cu, Zn, Co, Mg, Cr...) by the trivalent metals (Al, Fe, Tb...) and
68 it is neutralized by negatively exchangeable organic or inorganic ions (A = NO₃⁻, CO₃²⁻,
69 SO₄²⁻, F⁻, Cl⁻ or alkyl anions...) accompanied by the absorption of the interlayer water

71 molecules [7-12]. The remarkable advantages of the LDH are made of relatively
72 inexpensive and safe elements, highly adjustable, and easily synthesized that becomes
73 good advantages for industrial-scale applications. The physicochemical characteristics
74 could be controlled by the flexible exchange of the chemical components of the metal
75 hydroxide-based layer or the functionalization of the exchangeable interlayer ions.
76 Based on the host lamellar structure and ionic exchangeable possibility, LDH has been
77 widely studied in applicable fields such as absorbents [12], prominent photoactive
78 catalysts [13, 14], energy conversion and storage [15], and drug delivery systems [16-
79 18], as a result of the modification of the trivalent metal. Moreover, the efficiency of the
80 catalytic characteristics of the LDH has been highlighted to study the organic reactions
81 such as aldol condensation [19], ethanol electro-oxidation [20], and dinitrogen fixation
82 [21]. Most of the cases depend on the catalytic possibility of the functional groups
83 existing between the ionic metal hydroxide layers. Particularly, single-atom Au-
84 intercalated NiFe LDH, Ce-doped MgAl LDH functionalized Au nanoparticles, or
85 polyoxometalate-intercalated LDH have revealed the optimal achievements for catalytic
86 applications [22-24].
87 The improvement of the typical physicochemical characteristics or enhancement of the
88 active sites by adjusting the interlayer trivalent or divalent metals of the LDH as well as
89 exchanging a functionalized interlayer component was widely investigated. However,
90 the challenge to figure out a suitable synthesis depends on the intrinsic property and size
91 of the functional-controlling substances. In this study, the $\text{Cs}_2\text{Mo}_6\text{Cl}_{14}$ (CMC) clusters
92 compound, with excellent redox and optical properties, has been selected as a catalytic
93 functionalized group to combine with the LDH. As is known, the basic concept of metal
94 atom cluster (MC) was first introduced by F. A. Cotton in 1964 to define a finite group

95 of the metal atoms (two or more) that are held together by metal-metal bonds and
96 surrounded by other nonmetal ligands [25]. Typically, the octahedral MC (M_6)
97 composed of the $\{M_6L_8^i\}^{4+}$ ($M = Mo, W, Re$) metallic cores ($L^i =$ inner ligand)
98 coordinating with apical ligands ($L^a = Cl, Br, I$ or $OCOC_nF_{2n+1}$) exhibits strong
99 absorption in both the ultraviolet (UV) and visible light ranges, resulting in a prominent
100 luminescent emission within the deep red/near-infrared (NIR) region [26-29]. In the
101 reduced form, the valence electron concentration (VEC) is equal to 24 electrons per the
102 $[M_6L_8^iL_6^a]^{2-}$ cluster unit that visibly displays a redox characteristic for the catalyst
103 application [30-32]. As previously reported, the excitation state of MC produces singlet
104 oxygen (1O_2) with a strong catalytic activity for the photoreduction applications has
105 been investigated [33]. However, the Mo_6 cluster in the bulk powder state is limited in
106 the applicability as well. Graphene oxide or h-BN are ones of the excellent candidates to
107 enhance the photocatalytic applicability of the Mo_6 cluster has a proven highly catalytic
108 efficiency for the hydrogen production from water [34], water purification [35],
109 synthesis of dimethyl carbonate from CO_2 and methanol [36] or photoreduction of
110 carbon dioxide into methanol [37]. A remarkable study has been progressing to
111 simultaneously combine the gold nanoparticles and the Mo_6 cluster on the graphene
112 oxide resulting in an excellent photoactive possibility for the degradation of rhodamine
113 B under visible light irradiation [38]. A few studies have continued to determine
114 efficient supporting materials for the catalytic-characterized MC with the expectation to
115 fabricate the heterogeneous nanostructured composite for photovoltaic,
116 nanobiotechnology, or energy-saving fields [27, 28].
117 The goal of this study is to focus on the photoactive and oxidation properties of the MC
118 on dye degradation after combined with an LDH neutral supporting material with only

119 high absorbability and recyclability. Indeed, among LDH, Zn/Al LDH (abbreviated as
120 LDH-1) exists a weak basic catalyst, and Zn also was the limiting species for the
121 photocatalytic reaction [39]. It was almost used as an efficient absorbent and/or support
122 for multifunctional catalysts. In this work, the new nanocomposite (abbreviated as
123 Mo₆@LDH-2) was prepared by the delamination of Zn₂Al LDH co-intercalated dodecyl
124 sulfate (abbreviated as LDH-2) in dimethylformamide and then introducing the as-
125 synthesized [Mo₆Clⁱ₈Cl^a₆]²⁻ cluster units. The initial octahedral structure of the Mo₆
126 cluster was not modified after incorporation into the LDH, as confirmed by the optical
127 properties. The Mo-O-Al/Zn chemical bonding between the Mo atoms of the
128 {Mo₆Clⁱ₈}⁴⁺ anion cluster core and the LDH was validated. The new Mo₆@LDH-2
129 nanocomposites were successfully fabricated by a quick, cheap, and reproducible
130 method with high and stable efficiency of the Mo₆ cluster units. Moreover, we have
131 demonstrated the catalytic activity of the Mo₆ cluster anion intercalated in the LDH on
132 the methylene blue.

133

134 **2. MATERIALS AND METHODS**

135 *2.1 Materials*

136 The Zn(NO₃)₂·6H₂O (99%) and Al(NO₃)₃·9H₂O (98%, pH= 2~4) were supplied from
137 Chameleon Reagent. Sodium n-dodecyl sulfate (CH₃(CH₂)₁₀CH₂OSO₃Na) was
138 purchased from the Kanto Chemical Company. The sodium hydroxide (NaOH, 5 mol/L)
139 was purchased from Nacalai Tesque. All chemicals were used without purification. The
140 deionized water with the conductance of 0.5·10⁻⁴ S/m was obtained using Water
141 Purifiers WG710 equipment at 25°C.

142

143 2.2 Methods

144 *Preparation of LDH-1 and LDH-2*

145 LDH-1 and LDH-2 were prepared by the co-precipitation method with the Zn and Al
146 ratio of about 2 [7, 40]. Fixed amounts of the $\text{Zn}(\text{NO}_3)_2 \cdot 6\text{H}_2\text{O}$ (0.02 mol) and
147 $\text{Al}(\text{NO}_3)_3 \cdot 9\text{H}_2\text{O}$ (0.01 mol) salts were simultaneously dissolved in 50 ml of deionized
148 water and agitated by a magnetic stirrer for 1 h to obtain a homogeneous solution.
149 Similarly, the transparent mixture solution containing the $\text{Zn}(\text{NO}_3)_2 \cdot 6\text{H}_2\text{O}$ (0.02 mol),
150 $\text{Al}(\text{NO}_3)_3 \cdot 9\text{H}_2\text{O}$ (0.01 mol) and sodium dodecyl sulfate (SDS) (0.01 mol) in 50 ml of
151 deionized water was used for the preparation of the LDH-2. The aqueous solution of
152 NaOH (5 M) was then used to titrate the mixed salt solution until the pH value reached
153 10. The solution was then agitated for 24 h at room temperature to increase the
154 crystallinity of the LDH. The precipitated product was purified by deionized water
155 several times until the pH was about 7. The collected solid powder was dried at 60°C for
156 24 h for further use.

157

158 *Synthesis of $\text{Mo}_6@$ LDH-1 and $\text{Mo}_6@$ LDH-2 nanocomposites*

159 The CMC cluster unit was prepared according to a procedure already reported that
160 combined the use of solid-state and solution chemistries [41, 42]. LDH-1 or LDH-2 (0.3
161 g) was dispersed in 140 ml of dimethylformamide (DMF) by ultrasonication for 1 h.
162 The yellow CMC cluster powder (0.06 g) was similarly dissolved in 60 ml of DMF
163 solution by ultrasonication. LDH-1 or LDH-2 and CMC cluster solutions were then
164 mixed and continually agitated for 24 h to improve the intercalation. The yellow-
165 colored product was separated and washed with DMF to eliminate the residual Mo_6

166 cluster, then dried at 60°C for 24 h for further characterizations. The experimentally
167 determined wt. % concentration of the CMC cluster powder in the Mo₆@LDH-1 and
168 Mo₆@LDH-2 nanocomposite was about 16.7 wt.%.

169

170 *2.3 Catalytic test*

171 The catalytic activity of the LDH and Mo₆@LDH samples was characterized by
172 measuring the degradation possibility of methylene blue (MB) in an aqueous solution.
173 The difference in the catalytic activity and adsorption-desorption isotherm was
174 evaluated through the tests for LDH-2 and Mo₆@LDH-2 (catalyst/MB = 20). The
175 investigation was performed on the solution containing 20 mg of a catalyst in 10 ml of
176 MB solution (20 mg/L) (catalyst/MB = 100) at room temperature without or with i) the
177 addition of the H₂O₂ solution (5% in ethanol, Sanwa Chemical Co., Ltd.), ii) irradiation
178 of ultraviolet (UV) light ($\lambda = 370$ nm) or iii) in the presence of both H₂O₂/UV system. A
179 source of the UV light was generated by a 300 W Xenon lamp (MAX-303, Asahi
180 Spectra Co., Ltd.). The MB degradable efficiency of the filtered catalyst-mixed MB
181 solution was confirmed by the UV-Vis absorption spectroscopy (V-650, Jasco). The
182 C/C₀ index was calculated based on the intensity ratio of the optical absorption peak at
183 664 nm of MB with and without the existence of the catalyst. The catalytic reaction rate
184 and the effect of H₂O₂ concentration on the degradation reaction of MB with and
185 without the UV light were investigated. For comparison, the catalytic test of the CMC
186 cluster alone was also carried out at the same Mo₆ cluster concentration (16.7 wt%) in
187 the Mo₆@LDH-2 nanocomposite.

188

189 *2.4 Characterizations*

190 The average hydrodynamic diameters and distribution of the LDH-2 and Mo₆@LDH-2
191 powders in water were measured by an ultrafine particle analyzer (Nanotrac NPA151 -
192 Nanotrac ULTRA, Microtrac Inc., USA) incorporated the controlled reference method
193 (CRM) in a dynamic light scattering instrument. The crystalline layered structure of the
194 samples was determined by powder X-ray diffraction (XRD) (SmartLab, RIGAKU, 40
195 kV and 30 mA) in the 2θ angle range from 1° to 50° for the bulk powder at the scan
196 speed of 1/ min with the Cu Kα radiation (λ = 1.54 Å). The optical absorbances of the
197 powders were measured by UV-Vis-NIR spectroscopy (V570, Jasco Corp.) in the
198 wavelength range of 220 to 2000 nm at the scan rate of 400 nm/min. Emission spectra
199 of the powder were obtained by high-performance fluorescence spectroscopy (JASCO
200 FP8500) connected to a Xenon lamp at the scan rate of 500 nm/min. The surface
201 morphology and the elemental composition were analyzed by field emission scanning
202 electron microscopy (FE-SEM, S4800, Hitachi High-Technologies Corp.) at 10 kV
203 coupled with an energy-dispersive X-ray (EDX) analysis device. High-resolution
204 observations of the powder were performed by a high-resolution transmission electron
205 microscopy (HRTEM) (JEOL JEM 2100F) equipped with an EDX analysis device.
206 Inductively coupled plasma optical emission spectrometry (ICP-OES, Agilent 720-ES)
207 coupled with ion-chromatography (Thermofisher Scientific ICS-1600) was used to
208 verify the element concentration. The typical chemical vibrations of the samples were
209 verified by Fourier transform infrared spectroscopy (FTIR) (Thermo scientific Nicolet
210 4700) in the wavenumber range from 4000 to 400 cm⁻¹. The nitrogen adsorption
211 isotherm according to the BET model of the LDH-2 and Mo₆@LDH-2 nanoparticles
212 was performed in saturated vapor pressure of about 100 kPa at the temperature of 140°C
213 for 2 days (BELSORP-max II, Microtrac BEL Corp.). Thermogravimetric analysis

214 (TGA) and differential thermal analysis (DTA) were carried out using a TG/DTA 6200
215 apparatus (SII, EXSTAR 6000, Hitachi, Japan) operated in an N₂ atmosphere at the
216 heating rate of 10/min. The electron binding energy spectra within the CMC and
217 Mo₆@LDH-Zn/Al were measured by X-ray photoelectron spectroscopy (XPS) (PHI
218 Quantera SXM (ULVAC-PHI)) using Al K α radiation at 20 kV and 5 mA and taken off
219 the angle of 45°. All binding energies were calibrated concerning the C 1s peak of the
220 adventitious carbon at 285 eV.

221

222 3. RESULTS AND DISCUSSION

223 **Figure 1a** shows the powder XRD patterns of the as-synthesized LDH-1, Mo₆@LDH-1,
224 LDH-2, and Mo₆@LDH-2 powders, and the characteristic peaks are observed. The
225 LDH-1 exhibits the typical characteristic of the LDH phase assigned to structure I. The
226 characteristic diffraction peaks (indexation in bracket) are located at 2 θ angles of 11.6°
227 (003), 23.4° (006), 34.5° (009) and 39° (015), 46° (018) corresponding to the basal
228 planes as claimed in previous reports [43]. Besides, the remarkable patterns of the ZnO
229 phase formed on the brucite-like sheets were also verified with the peaks at the 2 θ
230 angles of 32°, 34°, and 36° in this study [43]. In the case of Mo₆@LDH-1, it shows the
231 same lamellar structure with LDH-1 without the change in the XRD peak positions. The
232 basal plane spacing value of the 003 planes calculated by Bragg's law for LDH-1 is
233 about 0.9 nm which is too narrow to intercalate the CMC clusters with a size of 1.2 nm
234 [42]. For this reason, the dodecyl sulfate (DS) anion was selected to expand the space of
235 the metal hydroxide layers in LDH-1 to form LDH-2. The XRD result of LDH-2
236 illustrates that a new series of reflections of the (003), (006) and (009) planes of LDH-2
237 simultaneously appear at the lower 2 θ angle assigned to structure II and the d₀₀₃ spacing

238 value increases from 0.9 to 2.7 nm. In addition, LDH-2 still retained the original layered
239 structure as seen for structure I in LDH-1. This result confirmed the partial exchange of
240 NO_3^- anions by the 2 nm-sized dodecyl sulfate anions as seen in previous reports [43,
241 44]. Very interestingly, the intercalation in the CMC cluster causes a significant
242 reduction of peak intensity assigned to structure II of LDH-2 as seen in the XRD pattern
243 of $\text{Mo}_6@$ LDH-2. It could be suggested that a part of the DS intercalated LDH, which is
244 mixed with the Mo_6 cluster, becomes a poorly crystallized phase, or undergoes
245 exfoliation. Good interaction between the DMF molecules and dodecyl sulfate anions is
246 efficient to expand the basal space between the brucite-like layers of LDH-2 that assists
247 in the movement and intercalation of the Mo_6 cluster during the intercalation step. The
248 average hydrodynamic diameters and distributions of LDH-2 and $\text{Mo}_6@$ LDH-2 in water
249 are displayed in **Figure S1**. The average hydrodynamic diameter of LDH-2 reduces
250 from 0.5980 μm to 0.2815 μm for $\text{Mo}_6@$ LDH-2 corresponding to the broader size
251 distribution. This result is agreeable with the crystallinity reduction of the LDH phase as
252 claimed in the XRD pattern, resulting in a partial exfoliation. The BET surface areas of
253 LDH-2 of about 50.0 m^2/g and $\text{Mo}_6@$ LDH-2 of about 20.4 m^2/g were evaluated by the
254 nitrogen adsorption isotherm (**Fig. S2a**). The shape of the nitrogen adsorption isotherm
255 curves of LDH-2 and $\text{Mo}_6@$ LDH-2 is almost similar to the characteristic of the LDH.
256 That proves the retention of the layered structure of the LDH in $\text{Mo}_6@$ LDH-2 after the
257 partial exfoliation as suggested in the XRD pattern. The decrease of the adsorbed
258 volume agrees with the pore diameter distribution in **Figure S2b** which shows the
259 significant reduction of the small pore size in the range below 20 nm. The schematic
260 representation of the process to fabricate the LDH and the possible structure of its
261 nanocomposite based on the XRD pattern are illustrated in **Figure 1b**.

262 The HRTEM image of Mo₆@LDH-2 shows black areas assigned to the aggregated Mo₆
263 cluster anion (**Fig. 2a**). In the beginning, the CMC cluster dissociates in the solvent to
264 form the Cs⁺ cations and [Mo₆Cl₈Cl₆^a]²⁻ anions. Moreover, it is well known that the
265 [Mo₆Cl₈Cl₆^a]²⁻ anion is able to quickly exchange apical Cl ligands by water molecules
266 or hydroxyl anions to obtain [Mo₆Cl₈Cl_{6-(x+y)}(H₂O)_x(OH)_y]^{x-2} (x + y ≤ 6) clusters [45].
267 Indeed, the interlayer galleries of LDH are containing water molecules and hydroxyl for
268 balancing the positively charged surface, which can react with the apical Cl ligands.
269 Following a theoretical suggestion, we can assume that only the Mo₆ anion or neutral
270 compound can adsorb or deposit on the positive metal hydroxide surface of the LDH, so
271 in that case x = 0 or 1 and y = 0 to 5.

272 The layer structure of Mo₆@LDH-2 is confirmed in the STEM image and the
273 calculation of the basal spacing distance of about 5 nm as seen in Figures **2b** and **2c**.
274 STEM-EDX mapping of the Mo₆@LDH-2 nanocomposite confirms the existence of Mo
275 and Cl atoms as presented in **Figure 2d**.

276 In order to confirm the stability of the octahedral structure of the Mo₆ cluster in
277 Mo₆@LDH-2, the optical properties of the reflectance and the photoluminescence were
278 evaluated. It could be seen that LDH-1 and LDH-2 show a high optical absorption
279 below 400 nm while Mo₆@LDH-2 is composed of the adsorbing part of the Mo₆ cluster
280 below 400 nm and the LDH below 370 nm (**Fig. 3a**). This result confirms the retention
281 of the octahedral Mo₆ structure on the LDH. In **Figure 3b**, LDH-1 and LDH-2 normally
282 possess no photoluminescence in the NIR range while the Mo₆ cluster shows a strong
283 emission at 700 nm in the deep red/NIR region. However, the photoluminescent
284 intensity of the Mo₆ cluster is not strong in the spectrum of Mo₆@LDH-2, this is due to
285 the significant change in the apical halogen ligand of the CMC cluster. As known, the

286 photoluminescent property of the Mo₆ cluster is decreased when the apical halogen
287 ligands are replaced by H₂O molecules or hydroxyl anion [32, 41, 45].

288 The chemical bonding of the prepared compounds was verified by FT-IR spectroscopy
289 presented in **Figure 4**. In the FT-IR spectrum of LDH-1 appears a strong peak at 1385
290 cm⁻¹ that indicates for the NO₃⁻ linking existing in the basal spacing of the LDH. In
291 addition, the vibrational bands for Zn-O at 427 cm⁻¹, Zn-OH at 608 cm⁻¹ of the brucite-
292 like layers, O-H bending at 1650 cm⁻¹ and O-H stretching at the broadband of 3450 cm⁻¹
293 of the free inter-lamellar water molecules are observed. The FT-IR spectrum of LDH-2
294 shows the vibrational bands assigned to the dodecyl sulfate: i) C-H stretching
295 vibrational band of CH₂ at 2928 cm⁻¹ and CH₃ at 2854 cm⁻¹ from the alkyl chain and ii)
296 asymmetric stretching vibrational band at 1220 cm⁻¹ and symmetric stretching
297 vibrational band at 1059 cm⁻¹ originating from the OSO₃⁻ group [43]. The vibrational
298 signal of NO₃⁻ at 1385 cm⁻¹ in LDH-2 decreases after exchanged by DS anions. The FT-
299 IR spectrum of Mo₆@LDH-2 would be composed of the vibrational band of the LDH-2
300 and Mo₆ clusters. Following the typical band intensity for DS, the concentration of DS
301 is obviously reduced by an exchange of the Mo₆ cluster. It should be noted that new
302 peaks appear at 1654 cm⁻¹ that were properly related to the O-H bending vibrational
303 band of the H₂O free molecules with strong hydrogen bonding [46] as recognized in the
304 report of the [Mo₆Br₈Br₆]²⁻ cluster [47]. From this result, the hydrogen bonding could
305 be created between apical groups of the [Mo₆Cl₈Cl_{6-(x+y)}(H₂O)_x(OH)_y]^{x-2} clusters and
306 the free interlayer-adsorbed water molecules in the LDH.

307 **Figure 5** shows the TG, DTG, and DTA results of the LDH-1, LDH-2, and Mo₆@LDH-
308 2. The total mass loss was respectively, figured to be about 40 wt. %, 50 wt. % and 46
309 wt. % for LDH-1, LDH-2, and Mo₆@LDH-2 after heating to 800°C. The

310 thermogravimetric behavior (DTG) shows the mass loss with four steps in the
311 temperature range of 50-200 °C, 200-300 °C, 300-500 °C and 500-800°C for LDH-1, 50-
312 150, 150-250, 250-400 and 400-800°C for LDH-2, and 50-150, 150-320, 320-600 and
313 600-800°C for Mo₆@LDH-2. The weight loss in the first step indicates the release of the
314 interlayer water molecules adsorbed on the surface of the Zn²⁺/Al³⁺ ionic brucite-like
315 layers. Dehydroxylation and thermal degradation of the counter anion is realized at the
316 second decomposing step and, simultaneously, metal oxidation occurs with the
317 dehydroxylation of the brucite-like layers. The complete dehydroxylation occurs in the
318 temperature range of 500-800°C that destroys the brucite-like structure of the LDH. In
319 the last step, all the counter anions, which are strongly adsorbed on the metal oxide
320 crystallites, would be removed.

321 The DTA curves of LDH-2 almost display only an exothermic event because of the
322 quick decomposition of the dodecyl sulfate during the beginning steps. In contrast, the
323 DTA results of LDH-1 and Mo₆@LDH-2 show a similar endothermic event in the
324 second thermal decomposing step. In this step, the phase transformation starts to occur
325 and accelerates the melting process to destroy the crystallinity of the brucite-like layers
326 in the third decomposition step. In Mo₆@LDH-2, the surfactant concentration was
327 significantly reduced that did not affect the decomposition as seen in LDH-2. In the
328 third and fourth degradation steps, the performance of the metal oxide from the
329 dihydroxylation of the brucite-like layers also enhances the enthalpy of the thermal
330 event that linearly increases the endothermic value [43]. Interestingly, in the third
331 degradation step of the DTA curve of Mo₆@LDH-2, a clearly enhanced endothermic
332 peak appears at 450 °C due to the formation of molybdenum oxide caused by the
333 destruction of the Mo₆ octahedral structure.

334 **Figure 6a** summarizes the XPS spectra of the CMC and Mo₆@LDH-2. All the binding
335 energies were calibrated concerning the C1s peak of the adventitious carbon at 285 eV.
336 The binding energies of the Zn, Al, C, O, Cs, Mo, Cl, and S elements in the CMC and
337 Mo₆@LDH-2 powders are listed in **Table S1**. Interestingly, the Cs element was not
338 found in Mo₆@LDH-2, as presented in **Figure 6a**. As already explained, in the solvent,
339 the CMC cluster dissociated to 2 Cs⁺ and 1 [Mo₆Cl₈Cl₆]²⁻ ions and the Cs⁺ cation can
340 be kept by the exchangeable anion adsorbed on the LDH or Cl⁻ from CMC, which was
341 removed through the washing step. The binding energies of Zn 2p and Al 2p are
342 respectively assigned by the two peaks at 1022.3 eV (2p_{3/2}) and 1045.4 eV (2p_{1/2}) and a
343 peak of 74.7 eV that agrees with a previous study [48]. The dodecyl sulfate component
344 is confirmed by the appearance of the binding energy of the S2p at the peak of 169.1 eV.
345 It is important to verify the difference in the binding energy of the Mo and Cl
346 components in the Mo₆ cluster after intercalated into the LDH.

347 In **Figure 6b**, the Mo3d XPS spectrum of the CMC cluster shows peaks at 229.7 eV
348 (3d_{5/2}) and 232.8 eV (3d_{3/2}) assigned to the Mo²⁺ cation from the [Mo₆Cl₁₄]²⁻ cluster [36].
349 In the XPS spectrum of Mo₆@LDH-2, the Mo3d binding energy is recognized by the
350 peaks at 229.7 eV (3d_{5/2}) and 232.6 eV (3d_{3/2}) related to the Mo₆⁻ cluster [49, 50, 51].
351 Interestingly, one new peak at 234 eV (3d_{3/2}) indicating Mo-O appears in the
352 Mo₆@LDH-2 compound. It could be proof for the interaction between the Mo atom
353 from the Mo₆ cluster and O atom from the hydroxalate layers of the LDH to form the
354 Mo-O-Zn or Mo-O-Al bonding. This behavior has been also claimed by Haiping Li et al.
355 for the Zn(Al)-O-Bi(Mo) bonds between the Bi₂MoO₆ groups and Zn/Al-LDH [52].
356 Moreover, the O1s XPS spectrum of Mo₆@LDH-2 shows a peak at 530.9 eV indicating
357 O-Mo bonding that was not confirmed in the XPS spectrum of the CMC cluster as

358 expected (**Tab. S1**). In addition, the binding energy assigned to the O1s of CMC with a
359 peak at 532.6 eV that is verified for the freely absorbed water molecules (**Tab. S1**)
360 while the binding energy of O1s of Mo₆@LDH-2 is also characterized by a peak at
361 530.9 eV which indicates the O-Zn, O-Al, or O-Mo bonding.

362 Similarly, the XPS spectrum of the CMC cluster for the Cl2p including three clear peaks
363 at 198.3 eV (2p_{3/2}), 200.4 (2p_{3/2}), and 200.2 (2p_{1/2}) while only one broad peak was
364 observed for the Cl2p for Mo₆@LDH-2 (**Fig. 6c**). To distinguish the inner and apical Cl
365 ligands, the spectrum deconvolution of the Cl2p region was performed for the XPS
366 spectra of the Cl2p of CMC cluster and Mo₆@LDH-2, as listed in Table 2. The
367 deconvolution spectrum of the Cl 2p region of the CMC cluster shows four peaks at
368 198.25, 199.85, 200.39 and 201.99 eV that indicate Cl^(a)2p_{3/2}, Cl^(a)2p_{1/2}, Cl⁽ⁱ⁾2p_{3/2} and
369 Cl⁽ⁱ⁾2p_{1/2}, respectively (**Fig. 6d and Tab. 1**) [53]. For Mo₆@LDH-2, the XPS
370 deconvolution of the Cl2p shows the same peaks at 198.25 eV (Cl^(a)2p_{3/2}), 199.85 eV
371 (Cl^(a)2p_{1/2}), 201.35 (Cl⁽ⁱ⁾2p_{3/2}), and 201.95 eV (Cl⁽ⁱ⁾2p_{1/2}) which are properly related to
372 Mo-Cl of the [Mo₆Clⁱ₈Cl^a₆]²⁻ anion (**Fig. 6e**). The ratio Cl^(a)2p/ Cl⁽ⁱ⁾2p was
373 experimentally calculated to be 5.8/8 for the [Mo₆Clⁱ₈Cl^a₆]²⁻ anion in the CMC cluster
374 and 3.6/8 for the [Mo₆Clⁱ₈Cl^a_{6-(x+y)}(H₂O)^a_x(OH)^a_y]^{x-2} anion in Mo₆@LDH-2. This
375 deconvolution agrees with an analysis of the XPS spectra as mentioned in Table 1,
376 following the average loss of at least three apical Cl ligands on the Mo₆ anion in
377 Mo₆@LDH-2. All these results support for the possible chemical bonding between the
378 [Mo₆Clⁱ₈Cl^a₃(OH)^a₃]²⁻ or [Mo₆Clⁱ₈Cl^a₃(H₂O)^a₃(OH)^a₂]⁻¹ anionic clusters or
379 [Mo₆Clⁱ₈Cl^a₃(H₂O)^a₂(OH)^a₁] neutral cluster and the hydroxide of ZnAL LDH. Very
380 interestingly, new peaks of the Cl2p were noted in the deconvolution spectrum at 198.9
381 eV (2p_{3/2}) and 200.5 eV (2p_{1/2}) that suggested the energy bonding of Cl with another

382 metal (Zn or Al) [48]. It could be explained that the apical Cl⁻ anions separated from the
383 Mo₆ cluster by exchange with the interlayer water molecules will directly adsorb on the
384 positively charged hydrotalcite surface of the LDH. Aiming to clarify the quantitative
385 analysis of the element components of Mo₆@LDH-2, an ICP-OES analysis was
386 performed that indicated the ratio of Zn, Al, and Mo atoms of about 1.96, 1.00, and 0.38.
387 The Mo element definitely existed in the Mo₆@LDH-2 at a significant concentration as
388 well as confirmed in the STEM-EDX mapping image. The ratio between the Cl and Mo
389 atoms in Mo₆@LDH-2 indicated by ICP-OES analysis was 2.23 (the theoretical ratio is
390 2.33) which means almost all the original Cl (from ligands) still exist in the
391 nanocomposite after treatment. This result suggests too that a part of the Cl⁻ could be
392 directly adsorbed on the LDH.

393 As known, the H₂O₂/UV or H₂O₂/catalyst systems are widely used in advanced
394 oxidation technology, one of the most environmentally friendly techniques to degrade
395 pollutants [54]. In this study, the efficiency of the MB degradation caused by the Mo₆
396 cluster deposited on LDH with and without UV and H₂O₂ or both as a radical generating
397 source. **Table S2** and **Figure 7** present the change in the C/C₀ value that was calculated
398 from the optical absorbance (664 nm) of the samples and blank illustrated in **Figure S3**.
399 First, the evaluation of the MB adsorbing possibility of LDH-2 and Mo₆@LDH-2 was
400 performed by stirring with MB aqueous solution (catalyst/MB = 20/1) for 72h in the
401 dark (**Fig. S3a**). The intensity of the adsorbing peak at 664 nm assigned to MB
402 significantly decreased by about 80 wt% caused by Mo₆@LDH-2, meanwhile, it is 66
403 wt% for LDH-2. Considering the BET surface area of LDH-2 of about 50.0 g/m² and
404 Mo₆@LDH-2 of about 20.4 g/m² (**Fig. S2**), the adsorbing possibility of the Mo₆@LDH-
405 2 should be lower than that of LDH-2. That means a part of the degraded MB is caused

406 by the oxidation reaction of the Mo₆ cluster. To clarify this phenomenon, the Mo₆ cluster,
407 LDH-2, Mo₆@LDH-2 powders were dispersed in the MB solution (catalyst/MB = 20/1)
408 in the dark, with UV or H₂O₂ or both of them for 2 h (**Fig. S3b and c**). The calculated
409 C/Co value of all samples was presented in **Figure 7a** and **Table S2**.

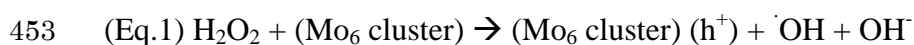
410 In **Figure 7a**, the decrease in the degraded MB concentration caused by the CMC
411 cluster was recorded at 57% in the dark, at 98% with UV or H₂O₂ that proved strong
412 oxidation and photoactive properties of the Mo₆ cluster [30, 31]. As a result,
413 Mo₆@LDH-2 also displays the MB degrading efficiency that is 71 wt% in dark and
414 96% with H₂O₂. Their MB degrading possibility slightly reduce in the irradiation of the
415 UV light for the same catalyst. This result is proof for the advantage of the intercalation
416 of the Mo₆ cluster on the LDH in comparison with LDH that shows the degraded MB
417 concentration at 54% in the dark and 65% with H₂O₂. Barras et al. reported the
418 photocatalytic degradation of rhodamine B over [Mo₆Br₈(N₃)₆]²⁻ cluster units under
419 sunlight irradiation with catalyst/rhB ratio of 1/1 for 2 h [38]. Besides, Ivanova et al.
420 also claimed the efficient photocatalyst of the hexamolybdenum cluster supported on
421 exfoliated hexagonal boron nitride (h-BN) nanosheet with the catalyst/rhB ratio of
422 100/1 [35]. In comparison, the H₂O₂/Mo₆@LDH system also shows a catalytic
423 efficiency with the catalyst/MB ratio of 100/1 even in the dark.

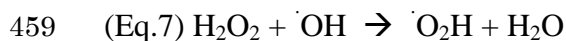
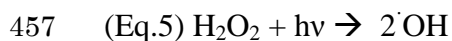
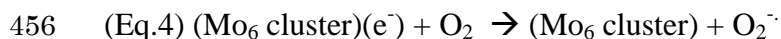
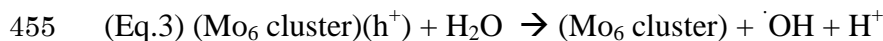
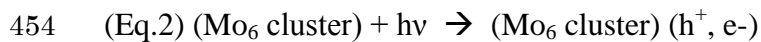
424 For the first time, the combination of the Mo₆ cluster and H₂O₂ was performed to test
425 the oxidation reaction on dye degradation and it shows excellent results. Only H₂O₂ is
426 unable to degrade the MB cations. H₂O₂ is suggested as an effective agent accelerating
427 for the Mo₆ cluster in the initial step of the MB degradation process.

428 **Figure 7b and 7c** illustrate the degradation rate and effect of the H₂O₂ concentration on
429 the catalytic activity of the H₂O₂/Mo₆@LDH-2 with and without UV ($\lambda=370$ nm) light

430 illumination as well as the change in the solution color as seen in **Figure S4**. The tested
431 suspensions were collected every 30 minutes from the original suspension for 210
432 minutes. The catalytic activity for the MB degradation decreases when the H₂O₂
433 concentration is increased. For this result, a suitable amount of H₂O₂ for the 20 mg
434 catalyst to obtain the optimal catalytic activity is recorded at 0.3 mM in both cases with
435 and without UV light illumination. The rate of the MB degradation by the H₂O₂/
436 Mo₆@LDH-2 is also confirmed with the strong reduction of the MB concentration for
437 the first 30 min that includes the absorption of MB on the surface of the LDH. The pH
438 increases, which is recorded during light irradiation, suggests the appearance of
439 hydroxyl anions during the initial and propagating reactions. Moreover, the chemically
440 component modification of the Mo₆@LDH-2 nanocomposite after the reaction with MB
441 in the presence of the H₂O₂ solution was measured by FTIR spectroscopy as seen in
442 **Figure S5**. The vibrational band assigned to the NO₃⁻ group was significantly decreased
443 accompanying a decrease in the O-H vibrational band assigned to the free H₂O
444 molecules that prove the use of interlayer-absorbed H₂O₂ molecules for the degradation
445 reaction of MB. Nevertheless, the XRD patterns of the Mo₆@LDH-2 before and after
446 the test with the MB degradation show no change as seen in **Figure S6**. That means the
447 layered structure of LDH is not modified and the degradation of the MB almost occurs
448 mostly on the outside surface of the Mo₆@LDH-2 nanosheets. In addition, the MB
449 degradable possibility by Mo₆@LDH-2 was observed for the concentration reduction of
450 about 66% for the second recycling run.

451 In summary, the non-photochemical reactions for the degradation of MB based on the
452 Mo₆@LDH-2 nanocomposite is suggested by the following equations [36, 37, 38, 55].





460 The Mo_6 cluster plays an important role as an electron supplying source for the initial
461 reaction with the strong support of H_2O_2 to generate free radicals as seen in Eq. 1. The
462 radical generating process is less efficient when the Mo_6 cluster is excited by UV light
463 because of taking two steps as depicted by Eq. 2 and Eq. 3 to form hydroxyl radicals
464 ($\cdot\text{OH}$), and Eq. 4 to form superoxide radical ($\text{O}_2^{\cdot-}$). For this reason, $\text{Mo}_6@LDH-2$ with
465 H_2O_2 presents a higher catalytic activity than $\text{Mo}_6@LDH-2$ with UV light. During the
466 initiating process by $\text{Mo}_6@LDH-2$ with H_2O_2 and UV light, the Eq. 5 and Eq. 6 site
467 reactions could significantly occur to reduce the H_2O_2 . The degradation rates of the
468 pollutants will decrease with the increase in the H_2O_2 concentration despite Eq. 7. The
469 generated hydroxyl radical can randomly attack the MB organic compound by hydrogen
470 abstraction, electron transfer, and radical combination to form the oxidation products
471 [56].

472 The representation of the structure and activity mechanism of $\text{Mo}_6@LDH-2$ for the
473 degradation of MB is illustrated in **Figure 8**. The efficiency of the catalytic activity
474 depends on the generation of highly reactive radicals and the stability of the radicals.
475 Without the light irradiation, ZnAl-LDH acts as a weak basic catalyst with the

476 hydroxide group the surface. ZnAl-LDH did not show the photocatalytic possibility due
477 to the weak performance of the Zn metal in the photocatalytic reaction [39]. In addition,
478 dye degradation was caused by the photocatalytic and oxidizing reactions. As a result,
479 the catalytic property of the Mo₆@LDH-2 was mostly originated from the photoactive
480 and oxidizing Mo metal cluster and the absorption caused by LDH. In the reduced form,
481 the valence electron concentration (VEC) occupying in the d orbitals of the six Mo
482 atoms, is equal to 24 electrons per Mo₆ cluster unit and it is reduced by a strong
483 oxidizing agent [31]. Moreover, a chemically and an electrochemically reversible
484 system has been reported. The Mo₆ cluster unit also provides one electron when excited
485 by the light and transfer to O₂ to form singlet oxygen (¹O₁) thus exhibiting a powerful
486 oxidant property [30, 32]. It could be summarized in this study that i) the reducing form
487 of the Mo₆ cluster can oxidize the MB molecules, ii) the Mo₆ cluster can combine with
488 H₂O₂ to create powerful, oxidizing hydroxides (OH[•]), ii) the Mo₆ cluster can be excited
489 by the UV light to form the hole and electron pair on the photoexcited cluster which
490 reacts with H₂O molecules to create the OH[•] radicals, and superoxide radical (O₂^{•-}),
491 particularly, singlet oxygen (¹O₁) as a powerful oxidant caused by photoluminescence
492 [36,37,38]. The oxygen-based radicals will first attack the C=S+-C linking of the MB
493 molecule existing on the surface of the LDH. A degradation mechanism of MB caused
494 by the oxygen-based radical is reported to form hydroxylation and oxidation products in
495 a previous study [57]. To understand the impact of the UV light on the catalytic reaction,
496 we consider some possible reasons. The UV light at 370 nm was used with the purpose
497 to optimally create the ¹O₁, O₂^{•-} and OH[•] oxygen-based radicals on the Mo₆ cluster which
498 directly react with MB. Unfortunately, from Figure 3, the UV light at 370 nm is partially
499 absorbed by the Zn-Al hydroxide layers that cause the decrease of the excitation photon

500 used for the Mo₆ cluster. In addition, the hole in the photoexcited Mo₆ cluster also reacts
501 with water to form protons which reduce the concentration of the OH[•] radicals. In the
502 catalyst with the H₂O₂/UV system, the H₂O₂ molecules could be degraded by the UV
503 energy. For this reason, the UV light will negatively affect the MB reducing the
504 efficiency of the Mo₆ cluster when UV light and H₂O₂ are used at the same time. In
505 summary, the prominent catalytic activity of the Mo₆ cluster stabilized on ZnAl-LDH
506 has been confirmed. The combination of the LDH with high absorbability and the
507 recyclability and the chemically reserving Mo₆ cluster will be a promising candidate as
508 a homogeneous catalyst for gas reactions with a strong selection based on the layer
509 structure.

510

511 **4. CONCLUSIONS**

512 A heterogeneous nanocomposite of ZnAl-LDH functionalized with the molybdenum
513 octahedral cluster (~ 16.7 wt. %) was successfully synthesized by the precipitation and
514 anion exchanging method under ambient conditions. The partially exfoliated ZnAl-
515 LDH functionalized with the Mo₆ cluster was carried out. The interaction between the
516 Mo₆ clusters and ZnAl-LDH is suggested to be via hydrogen bonding and/or new Mo-
517 O-Al/Zn covalent linkage. The photoactive and oxidation of the Mo₆ cluster in the
518 Mo₆@LDH nanocomposite present the important role to degrade methylene blue (MB).
519 This point was investigated under UV ($\lambda = 370$ nm), in the presence of H₂O₂, or both of
520 UV and H₂O₂ as radical initial agents. The efficiency of the degradation of MB using
521 the Mo₆@LDH-2 nanocomposite is evaluated at more than about 90 wt% after 2 h with
522 H₂O₂ as optimal co-agent. These results proved that the octahedral Mo₆ clusters are
523 efficiently retained on the brucite-like layers that provide new heterogeneous catalytic

524 materials' family for gas reactions in the future.

525

526 ACKNOWLEDGMENT

527 These studies were carried out as a part of the France-Japan International Collaboration
528 Framework (UMI3629 LINK). The authors wish to thank Mr. D. Lechevalier and Dr. M.
529 Zhou of Saint-Gobain KK (Tokyo, Japan) and Dr. D. Berthebaud of CNRS for their
530 many supports involved in LINK and related activities. We also wish to thank Dr. C.
531 Zhang at NIMS for his help with the EPD experiments, Dr. A. Iwanade at NIMS for his
532 help with the ICP-OES measurement and Dr. H. Ohata at NIMS for his help with the
533 XPS measurements.

534

535 APPENDIX A. SUPPLEMENTARY MATERIAL

536 Supplementary data to this article can be found online at

537

538 REFERENCES

- 539 1. Pirila, M., Drault, F., Keiski, R.L., Saouabe, M., Valtanen, A., Ojala, S., Huuhtanen,
540 M., Rathnayake, B., Brahmi, R., 2015. Photocatalytic Degradation of Organic Pollutants
541 in Wastewater. *Top Catal.* 58, 1085-1099.
- 542 2. Bagheri, S., Yousefi, A.T., Do, T.O., 2017. Photocatalytic pathway toward
543 degradation of environmental pharmaceutical pollutants: structure, kinetics and
544 mechanism approach, *Catal. Sci. Technol.*, 7, 4548–4569.
- 545 3. Fanourakis, S.K., Peña-Bahamonde, J., Bandara, P.C., Rodrigues, D.F., 2020. Nano-
546 based adsorbent and photocatalyst use for pharmaceutical contaminant removal during

547 indirect potable water reuse, *npj Clean Water*, 3, 1-15.

548 4. Mohapatra, L., Parida, K., 2016. A review on the recent progress, challenges and
549 perspective of layered double hydroxides as promising photocatalysts, *J. Mater. Chem.*
550 *A*, 4, 10744-10766.

551 5. Chubar, N., Gilmour, R., Gerda, V., Mičušík, M., Omastova, M., Heister, K., Man, P.,
552 Fraissard, J., Zaitsev, V., 2017. Layered double hydroxides as the next generation
553 inorganic anion exchangers: Synthetic methods versus applicability, *Adv. Colloid and*
554 *Inter. Sci.* 245, 62-80.

555 6. Meng, Z., Zhang, Y., Zhanga, Q., Chena, X., Liua, L., Komarneni, S., Lva, L., 2017.
556 Novel synthesis of layered double hydroxides (LDHs) from zinc hydroxide, *App. Surf.*
557 *Sci.* 396, 799-803.

558 7. Ahmed, A. A. A., Tali, Z. A., Hussein, M. Z., Zakaria, A., 2012. Zn–Al layered double
559 hydroxide prepared at different molar ratios: Preparation, characterization, optical and
560 dielectric properties, *J. Solid State Chem.* 191, 271-278.

561 8. Kim, S. J., Lee, Y., Lee, D. K., Lee, J. W., Kang, J.K., 2014. Efficient Co–Fe layered
562 double hydroxide photocatalysts for water oxidation under visible light, *J. Mater. Chem.*
563 *A*, 2, 4136-4139.

564 9. Chowdhury, P. R., Bhattacharyya, K. G., 2015. Synthesis and characterization of
565 Co/Ti layered double hydroxide and its application as a photocatalyst for degradation of
566 aqueous Congo Red, *RSC Adv.* 5, 92189-92206.

567 10. Zheng, Y., Chen, Y., 2017. Preparation of polypropylene/Mg–Al layered double
568 hydroxides nanocomposites through wet pan-milling: formation of a second-staging
569 structure in LDHs intercalates. *RSC Adv.* 7, 1520-1530.

570 11. Fu, Y., Ning, F., Xu, S., An, H., Shao, M., Wei, M., 2016. Terbium doped ZnCr-

571 layered double hydroxides with largely enhanced visible light photocatalytic
572 performance, *J. Mater. Chem. A* 4, 3907-3913.

573 12. Ma, L., Wang, Q., Islam, S. M., Liu, Y., Ma, S., Kanatzidis, M. G., 2016. Highly
574 selective and efficient removal of heavy metals by layered double hydroxide
575 intercalated with the MoS_4^{2-} ion, *J. Am. Chem. Soc.* 138, 2858–2866.

576 13. Fan, G., Li, F., Evans, D. G., Duan, X. 2014. Catalytic applications of layered
577 double hydroxides: recent advances and perspectives, *Chem. Soc. Rev.* 43, 7040-7066

578 14. Wu, M. J., Wu, J. Z., Zhang, J., Chen, H., Zhou, J. Z., Qian, G. R., Xu, Z. P., Dud, Z.,
579 Rao, Q. L., 2018. A review on fabricating heterostructures from layered double
580 hydroxides for enhanced photocatalytic activities, *Catal. Sci. Technol.* 8,1207-1228.

581 15. Patel, R., Park, J. T., Patel, M., Dash, J. K., Gowd, E. B., Karpoomath, R., Mishra,
582 A., Kwak, J., Kim, J. H., 2018. Transition-metal-based layered double hydroxides
583 tailored for energy conversion and storage, *J. Mater. Chem. A* 6, 12-29.

584 16. Barahuie, F., Hussein, M.Z., Arulselvan, P., Fakurazi, S., Zainal, Z., 2014. Drug
585 delivery system for an anticancer agent, chlorogenate-Zn/Al-layered double hydroxide
586 nanohybrid synthesised using direct co-precipitation and ion exchange methods, *J. Solid*
587 *State Chem.* 217, 31-41.

588 17. Fontes, D.A.F., Lyra, M.A.M., Andrad, J. K. F., Schver, G. C. R., Rolim, L.A., Silva,
589 T. G., Soares-Sobrinho, J.L., Alves-Junior, S., Rolim-Neto, P.J., 2016. CaAl-layered
590 double hydroxide as a drug delivery system: effects on solubility and toxicity of the
591 antiretroviral efavirenz, *J. Incl. Phenom. Macrocycl. Chem.*, 85, 281-288.

592 18. Kura, A.U., Hussein, M.Z., Fakurazi, S., Arulselvan, P., 2014. Layered double
593 hydroxide nanocomposite for drug delivery systems; bio-distribution, toxicity and drug
594 activity enhancement, *Chem. Central J.* 8, 47-55.

- 595 19. Sahoo, M., Singha, S., Parida, K. M., 2011. Amine functionalized layered double
596 hydroxide: a reusable catalyst for aldol condensation, *New J. Chem.* 35, 2503-2509.
- 597 20. Shao, M., Ning, F., Zhao, J., Wei, M., Evans, D.G., Duan, X., 2013. Hierarchical
598 layered double hydroxide microspheres with largely enhanced performance for ethanol
599 electrooxidation, *Adv. Funct. Mater.* 23, 3513-3518.
- 600 21. Zhao, Y., Zhao, Y., Waterhouse, G. I .N., Zheng, L., Cao, X., Teng, F., Wu, L. Z.,
601 Tung, C.H., O'Hare, D., Zhang, T., 2017. Layered-Double-Hydroxide nanosheets as
602 efficient visible-light-driven photocatalysts for dinitrogen fixation, *Adv. Mater.* 29,
603 1703828-1703838.
- 604 22. Zhang, j., Liu, J., Xi, L., Yu, Y., Ning Chen, .N, Sun, S., Wang, W., Lange, K.M.,
605 Zhang, B., 2018. Single-Atom Au/NiFe Layered Double Hydroxide Electrocatalyst:
606 Probing the Origin of Activity for Oxygen Evolution Reaction, *J. Am. Chem. Soc.*, 140,
607 3876–3879.
- 608 23. Iqbal, K., Iqbal, A., Kirillov, A.M., Wang, B., Liu, W., Tang, Y., 2017. A new Ce-
609 doped MgAl-LDHs@Au nanocatalyst for highly efficient reductive degradation of
610 organic contaminants. *J. Mater. Chem. A*, 5, 6716 –6724.
- 611 24. Liu, J.C., Qi, B., Song, I.F., 2020, Engineering polyoxometalate-intercalated layered
612 double hydroxides for catalytic applications, *Dalton Trans.*, 49, 3934–3941.
- 613 25. Cotton, F.A., 1964. Metal Atom Clusters in Oxide Systems. *Inorg. Chem.* 3, 1217-
614 1220.
- 615 26. Nguyen, T. K. N., Renaud, A., Bierre, B., Bouteille, B., Wilmet, M., Dubernet, M.,
616 Ohashi, N., Grasset, F., Uchikoshi, T. Extended Study on Electrophoretic Deposition
617 Process of Inorganic Octahedral Metal Clusters: Advanced Multifunctional Transparent
618 Nanocomposite Thin Films, *Bull. Chem. Soc. Jpn.*, 2018, 91, 1763-1774.

619 27. Neaime, C., Amela-Cortes, M., Grasset, F., Molard, Y., Cordier, S., Dierre, B.,
620 Mortier, M., Takei, T., Takahashi, K., Haneda, H., Verelst, M., Lechevallier, S., 2016.
621 Time-gated luminescence bioimaging with new luminescent nanocolloids based on
622 $[\text{Mo}_6\text{I}_8(\text{C}_2\text{F}_5\text{COO})_6]^{2-}$ metal atom clusters, *Phys. Chem. Chem. Phys.* 18, 30166-30173.

623 28. Efremova, O.A., Brylev, K.A., Vorotnikov, Y.A., Vejsadova, L., Shestopalov, M.A.,
624 Chimonides, G.F, Mikes, P., Topham, P.D., Kim, S.J., Kitamura, N., Sutherland, A.J.,
625 2016. Photoluminescent materials based on PMMA and a highly-emissive octahedral
626 molybdenum metal cluster complex. *J. Mater. Chem. C*, 4, 497-503.

627 29. Kirakci, K., Kubát, P., Dusek, M., Fejfarová, K., Sícha, V., Mosinger, J., Lang, K.,
628 2012. A Highly Luminescent Hexanuclear Molybdenum Cluster—A Promising
629 Candidate toward Photoactive Materials, *Eur. J. Inorg. Chem.* 19, 3107-3111.

630 30. Kirakci, K., Kubát, P., Langmaier, J., Polívka, T., Fuciman, M., Fejfarová, K., Lang,
631 K.A., 2013. Comparative study of the redox and excited state properties of
632 $(\text{nBu}_4\text{N})_2[\text{Mo}_6\text{X}_{14}]$ and $(\text{nBu}_4\text{N})_2[\text{Mo}_6\text{X}_8(\text{CF}_3\text{COO})_6]$ ($\text{X} = \text{Cl}, \text{Br}, \text{or I}$), *Dalton Trans.*
633 42, 7224-7232.

634 31. Vorotnikova, N.A., Vorotnikov, Y.A., Novozhilov, I. N., Syrokvashin, M.M.,
635 Nadolnny, V.A., Kuratieva, N.V., Benoit, D.M., Mironov, Y.V., Walton, R.I., Clarkson,
636 G.J., Kitamura, N., Sutherland, A.J., Shestopalov, M.A., Efremova, O.A., 2018.
637 ²³Electron Octahedral Molybdenum Cluster Complex $[\{\text{Mo}_6\text{I}_8\}\text{Cl}_6]^-$, *Inorg. Chem.* 57,
638 811–820.

639 32. Costuas, K., Bulou, A.A., Fontaine, B., Cuny, J., Gautier, R., Mortier, M., Molard, Y.,
640 Duvail, J.L., Faulques, E., Cordier, S., 2015. Combined theoretical and time-resolved
641 photoluminescence investigations of $[\text{Mo}_6\text{Br}^i_8\text{Br}^a_6]$ metal cluster units: evidence of dual
642 emission, *Phys. Chem. Chem. Phys.* 17, 28574-28585.

643 33. Jackson, J.A., Turro, C., Newsham, M.D., Nocera, D.G., 1990. Oxygen Quenching
644 of Electronically Excited Hexanuclear Molybdenum and Tungsten Halide Clusters, J.
645 Phys. Chem. A. 94, 4500-4507.

646 34. Feliz, M., Puche, M., Atienzar, P., Concepci n, P., Cordier, S., Molard, Y., 2016. In
647 Situ Generation of Active Molybdenum Octahedral Clusters for Photocatalytic
648 Hydrogen Production from Water, Chem. Sus. Chem. 9, 1963-1971.

649 35. Ivanova, M.N., Vorotnikov, Y.A., Plotnikova, E.E., Marchuk, V.M., Ivanov, A.A.,
650 Asanov, I.P., Tsygankova, A.R., Grayfer, E.D., Fedorov, V.E., Shestopalo, M.A., 2020,
651 Hexamolybdenum Clusters Supported on Exfoliated h-BN Nanosheets for
652 Photocatalytic Water Purification, Inorg. Chem., 59, 6439-6448.

653 36. Kumar, S., Khatri, O. P., Cordier, S., Boukherroub, R., Jain, S.L., 2015. Graphene
654 Oxide Supported Molybdenum Cluster: First Heterogenized Homogeneous Catalyst for
655 the Synthesis of Dimethylcarbonate from CO₂ and Methanol, Chem. Eur. J. 21, 3488 -
656 3494.

657 37. Barras, A., Devarapallic, M.R., Shelke, R.R., Cordier, S., M.V., Szunerits, S.,
658 Boukherroub, R., 2013. One-pot synthesis of gold nanoparticle/molybdenum
659 cluster/graphene oxide nanocomposite and its photocatalytic activity, App. Cat. B: Envi.
660 270- 276, 130-131.

661 38. Barras, A., Cordier, S., Boukherroub, R., 2012. Fast photocatalytic degradation of
662 rhodamine B over [Mo₆Br₈(N₃)₆]²⁻ cluster units under sun light irradiation, Appl. Cat.
663 B: Envi. 123-124, 1- 8.

664 39. Yang, Y., Zhang, C., Zeng, G., Tan, X., Wang, H., Huang, D., Yang, K., Wei, J.,
665 Maab, C., Nie, K., 2020. Design and engineering of layered double hydroxide based
666 catalysts for water depollution by advanced oxidation processes: a review, J. Mater.

667 Chem. A 8, 4141–4173.

668 40. Starukh, G., 2017. Photocatalytically enhanced cationic dye removal with Zn-Al
669 layered double hydroxides. *Nanoscale Research Lett.* 12, 391-399.

670 41. Saito, N., Lemoine, P., Dumait, N., Amela-Cortes, M., Paofai, S., Roisnel, T., Nassif,
671 V., Grasset, F., Wada, Y., Ohashi, N., Cordier, S., 2017. From $\text{Cs}_2\text{Mo}_6\text{Cl}_{14}$ to
672 $\text{Cs}_2\text{Mo}_6\text{Cl}_{14}$ center dot H_2O and Vice Versa: Crystal Chemistry Investigations, *J. Clust.*
673 *Sci.* 28, 773-798.

674 42. Kirakci, K., Cordier, S., Perrin, C., 2005. Synthesis and characterization of
675 $\text{Cs}_2\text{Mo}_6\text{X}_{14}$ (X = Br or I) hexamolybdenum cluster halides: Efficient Mo_6 cluster
676 precursors for solution chemistry syntheses. *Z. Anorg. Allg. Chem.* 631, 411-416.

677 43. Deng, L., Zeng, H., Zhang, Z.W., Luo, J., Sodium dodecyl sulfate intercalated and
678 acrylamide anchored layered double hydroxides: A multifunctional adsorbent for highly
679 efficient removal of Congo red. *J. Colloid and Inter. Sci.* 521 (2018) 172-182.

680 44. Ahmed, A.A.A., Talib, Z.A., Hussein, M.Z., 2015. Influence of sodium dodecyl
681 sulfate concentration on the photocatalytic activity and dielectric properties of
682 intercalated sodium dodecyl sulfate into Zn–Cd–Al layered double hydroxide, *Mater.*
683 *Research Bulletin.* 62, 122-131.

684 45. Zarate, X., Schott, E., Soto, L.A., Tagle, R.R., 2013. A family of octahedral
685 molybdenum cluster complexes $[\text{Mo}_6\text{Cl}_8(\text{H}_2\text{O})_n(\text{OH})_{6-n}]^{n-2}$ with $n = 0-6$ as a pH-
686 sensors: A theoretical study, *Chem. Phys. Lett.* 567, 39-42.

687 46. Chuntunov, L., Kumar, R., Kuroda, D.G., 2014. Non-linear infrared spectroscopy of
688 the water bending mode: direct experimental evidence of hydration shell reorganization.
689 *Chem. Chem. Phys.*, 16, 13172-13181.

690 47. Nguyen, T.K.N., Dierre, B., Grasset, F., Renaud, A., Cordier, S., Lemoine, P.,

691 Ohashi, N., Uchikoshi, T. 2017. Formation mechanism of transparent Mo₆ metal atom
692 cluster film prepared by electrophoretic deposition, *J. Electrochem. Soc.*, 164, 412-418.
693 48. Richetta, M., Digiamberardino, L., Mattoccia, A., Medaglia, P.G., Montanari, R.,
694 Pizzoferrato, R., Scarpellini, D., Varone, A., Kaciulis, S., Mezzi, A., Soltania, P., Orsinid,
695 A., 2016. Surface spectroscopy and structural analysis of nanostructured multifunctional
696 (Zn, Al) layered double hydroxides, *Surf. Interface Anal.* 48, 514-518.
697 49. Galtayries, A., Wisniewski, S., Grimblot, J., 1997. Formation of thin oxide and
698 sulphide films on polycrystalline molybdenum foils: characterization by XPS and
699 surface potential variations. *J. Electron Spectroscopy and Related Phenomena*, 87, 31-
700 44.
701 50. Castañeda, S.I., Montero, I., Ripalda, J.M., Díaz, N., Galán, L., Rueda, F., 1999. X-
702 ray photoelectron spectroscopy study of low-temperature molybdenum oxidation
703 process, *J. Appl. Phys.* 85, 8415-8418.
704 51. Bamroongwongdee, C., Bowker, C. M.A.F., Davies, P. R., Davies, R. J., Edwards,
705 D., 2013. Fabrication of complex model oxide catalysts: Mo oxide supported on
706 Fe₃O₄(111), *Faraday Discuss*, 162, 201–212.
707 52. Li, H., Deng, Q., Liu, L., Hou, W., Du, N., Zhang, R., Tao, X., 2014. Synthesis,
708 characterization and enhanced visible light photocatalytic activity of Bi₂MoO₆/Zn–Al
709 ed double hydroxide hierarchical heterostructures, *Catal. Sci. Technol.* 4, 1028–1037.
710 53. Saito, N., Cordier, S., Lemoine, P., Ohsawa, T., Wada, Y., Grasset, F., Cross, J. S.,
711 Ohashi, N., 2017. Lattice and valence electronic structures of crystalline octahedral
712 molybdenum halide clusters-based compounds, Cs₂[Mo₆X₁₄] (X = Cl, Br, I), studied by
713 density functional theory calculations, *Inorg. Chem.* 56, 6234–6243.
714 54. Tijani, J.O., Fatoba, O.O., Madzivire, G., Petrik, L.F., 2014. A review of combined

715 advanced oxidation technologies for the removal of organic pollutants from water.
716 Water, Air, Soil & Pollution, 225, 2102-2148.
717 55. Gligorovski, S., Strekowski, R., Barbati, S., Vione, D., 2015. Environmental
718 implications of hydroxyl radicals ($\bullet\text{OH}$). Chem. Rev., 115, 13051–13092.
719 56. Munter, R., 2001. Advanced oxidation processes – current status and prospects. Proc.
720 Estonian Acad. Sci. Chem. 50, 59-80.
721 57. Xia, S., Zhang, L., Pan, G., Qiana, P., Ni, Z., 2015. Photocatalytic degradation of
722 methylene blue with a nanocomposite system: synthesis, photocatalysis and degradation
723 pathways. Phys. Chem. Chem. Phys., 17, 5345-5355.

724

725 **FIGURE CAPTIONS**

726 **Figure 1.** A) Powder-XRD patterns of LDH-1, $\text{Mo}_6\text{@LDH-1}$, LDH-2, $\text{Mo}_6\text{@LDH-2}$
727 with the indications of the planes of 003 (■), 006 (●), 009 (▲) and the lozenge symbol
728 (◆) assigned for the ZnO phase. B) The schematic representation of the process to
729 fabricate the LDH and designed structure of its nanocomposite.

730 **Figure 2.** A) The HR-TEM, B) STEM images of the layered structure, and C) profile of
731 spacing distance between the layers, and D) STEM-EDX mapping of the $\text{Mo}_6\text{@LDH-2}$
732 nanocomposite.

733 **Figure 3.** A) UV-Vis absorbance spectra and B) room temperature photoluminescence
734 spectra excited by 325 nm (He-Cd) laser of CMC cluster, LDH-1, LDH-2, and
735 $\text{Mo}_6\text{@LDH-2}$.

736 **Figure 4.** FTIR spectra of CMC cluster and $\text{Mo}_6\text{@LDH}$ nanocomposites.

737 **Figure 5.** Thermal analysis of LDH-1, LDH-2, and $\text{Mo}_6\text{@LDH-2}$

738 **Figure 6.** (A) XPS binding energy (eV) spectrum of the CMC powder and the

739 Mo₆@LDH-2 nanocomposite, XPS spectra of (B) Mo 3d, (C) Cl 2p region.

740 Deconvolution spectra of Cl 2p region of (D) the CMC and (E) Mo₆@LDH-2.

741 **Figure 7.** A) The MB-degradable possibility caused by (1) Mo₆ cluster, (2) Mo₆@LDH-

742 2, and (3) LDH-2 without and with H₂O₂ during stirring for 2 h, B) the degradation rate

743 and C) the effect of H₂O₂ concentrations on MB-degradable possibility by Mo₆@LDH-2

744 for 210 minutes with and without UV light ($\lambda=370$ nm) illumination.

745 **Figure 8.** Schematic representation of the heterogeneous activation mechanism of

746 Mo₆@LDH-2 initiated by UV ($\lambda=370$ nm) and H₂O₂ oxidation agents.

747

748

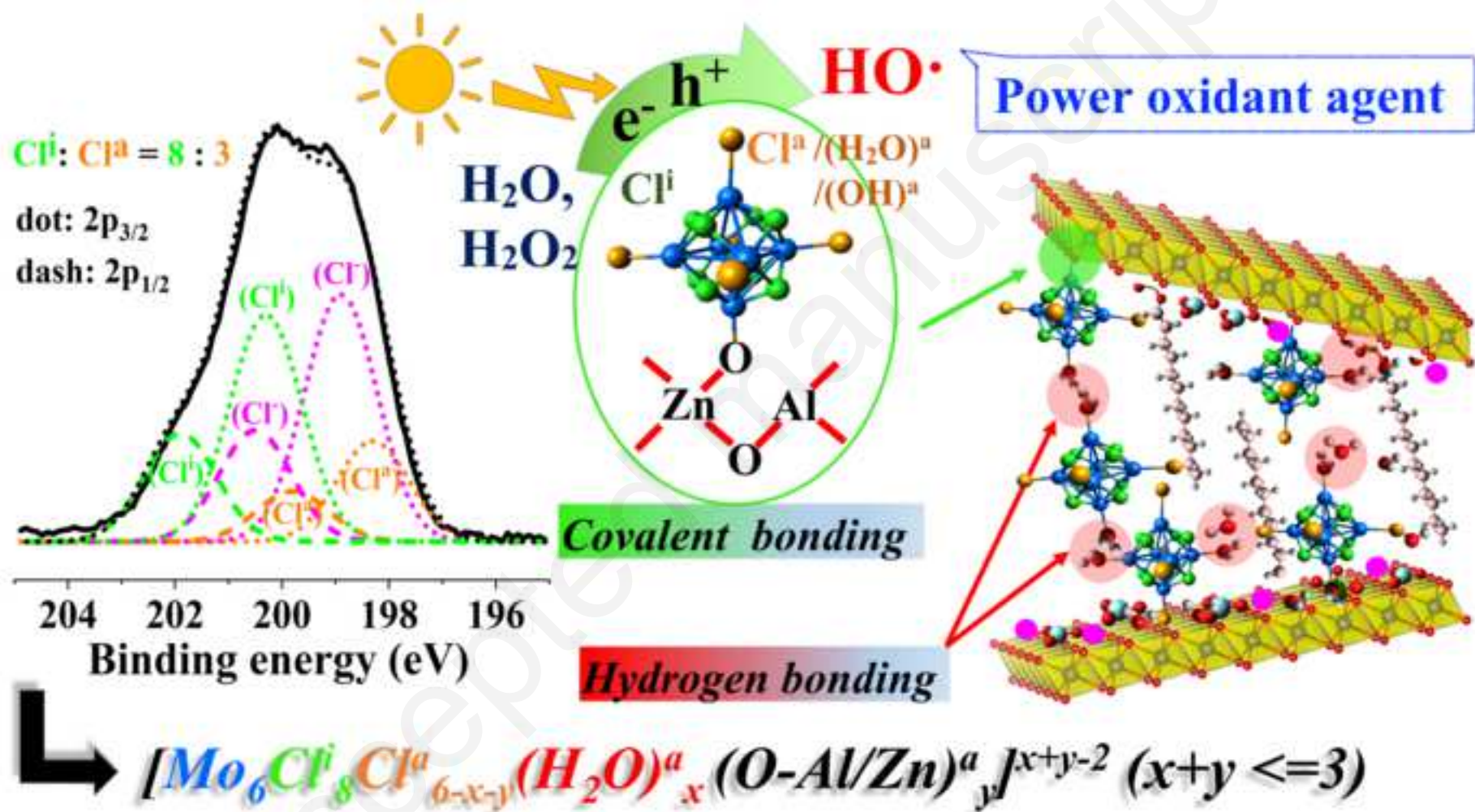
749 TABLES

750 Table 1. XPS binding energy (eV) of deconvolution spectra of Cl 2p region of the

751 [Mo₆Clⁱ₈Cl^a₆]²⁻ anions of CMC cluster and Mo₆@LDH-2.

752 Table 2. The concentration of the component elements in the CMC powder and the

753 Mo₆@LDH-2 nanocomposite by the peak analysis of the XPS measurements.



Highlights

ZnAl-LDHs were successfully functionalized with the hexamolybdenum cluster by covalent linkage.

A Mo₆@LDHs nanocomposite retains the photoactive and oxidation properties of the Mo₆ cluster

Three nanomaterial phases were found in the lamellar structure of the Mo₆@LDHs

H₂O₂/Mo₆@LDHs efficiently accelerated the degradation reaction of methylene blue with and without UV light illumination

TABLES

Table 1. XPS binding energy (eV) of deconvolution spectra of Cl 2p region of the $[\text{Mo}_6\text{Cl}_8\text{Cl}_6^{\text{a}}]^2$ anions of $\text{Cs}_2\text{Mo}_6\text{Cl}_{14}$ cluster and $\text{Mo}_6@LDH-2$.

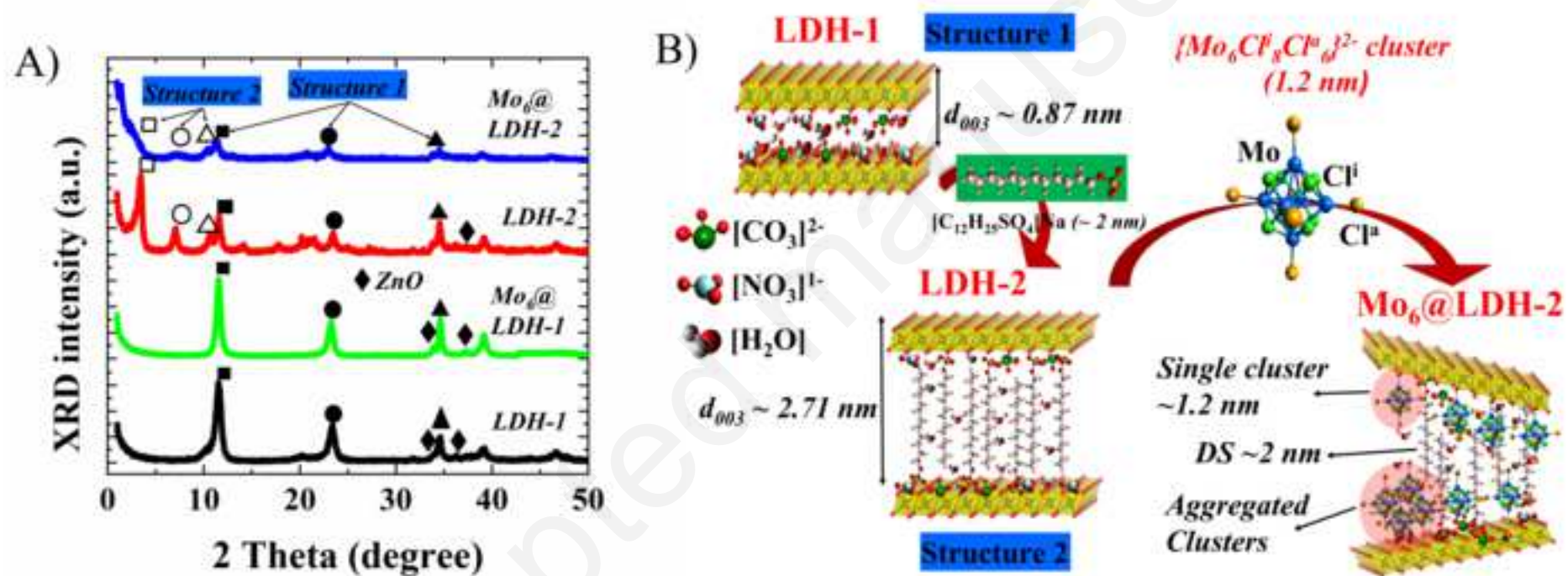
Sample	B.E	FWHM	Height	% area	Peak	$\text{Cl}^{\text{i}}/\text{Cl}^{\text{a}}/\text{Cl}^{\text{new}}$
$\text{Cs}_2\text{Mo}_6\text{Cl}_8\text{Cl}_6^{\text{a}}$	198.25	1.15	15637	27.88	Cl 2p _{3/2} (a)	8/5.8/0
	199.85	1.15	7895	14.08	Cl 2p _{1/2} (a)	
	200.39	1.16	21005	37.78	Cl 2p _{3/2} (i)	
	201.99	1.16	11265	20.26	Cl 2p _{1/2} (i)	
$\text{Mo}_6@LDH-2$	198.25	1.6	977	11.90	Cl 2p _{3/2} (a)	8/3.6/8.6
	198.90	1.6	2403	28.28	Cl 2p _{3/2}	
	199.85	1.6	488	5.95	Cl 2p _{1/2} (a)	
	200.35	1.6	2207	26.89	Cl 2p _{3/2} (i)	
	200.50	1.6	1081	13.17	Cl 2p _{1/2}	
	201.95	1.6	1051	12.81	Cl 2p _{1/2} (i)	

Table 2. The concentration of the component elements in the $\text{Cs}_2[\text{Mo}_6\text{Cl}_{14}]$ powder and the $\text{Mo}_6@LDH-2$ nanocomposite by the peak analysis of the XPS measurements.

Element component (% at.)	$\text{Cs}_2\text{Mo}_6\text{Cl}_{14}$	$\text{Mo}_6@LDH-2$
Al	0	3.8
Zn	0	12.4
S	0	1.5
C	28.5	29.1
O	5.2	47.3
Cl	42	3.8
Mo	17.7	2.1

Cs	6.6	0
Cs/ Mo/Cl	2.2/6.0/14.2	0/6.0/10.7

Accepted manuscript



Figure

[Click here to download high resolution image](#)

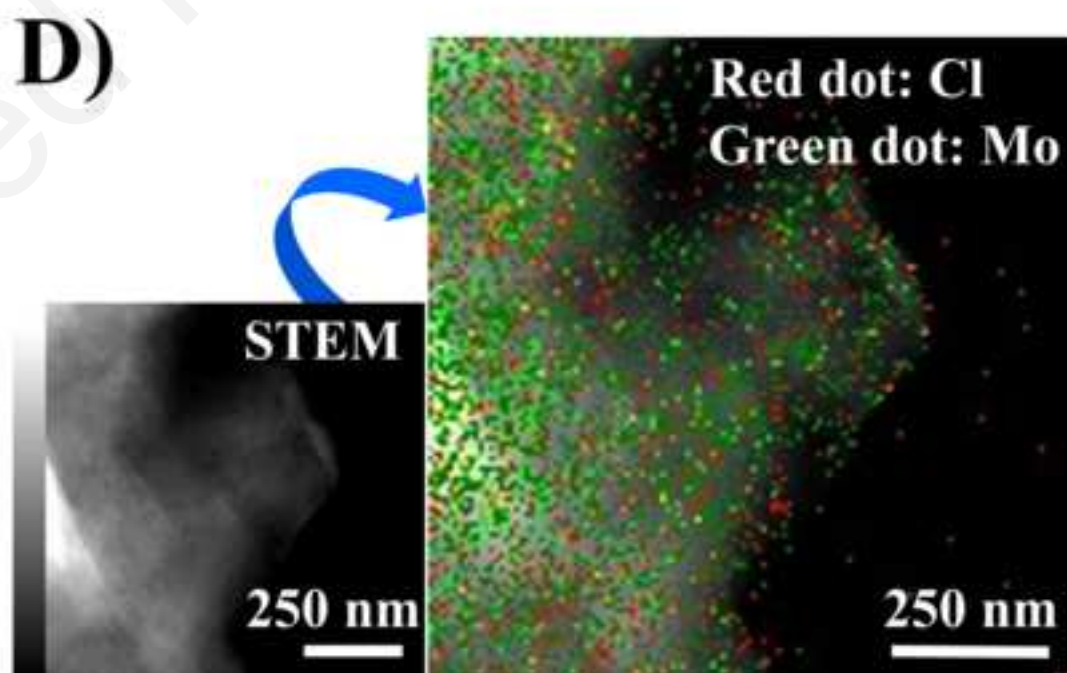
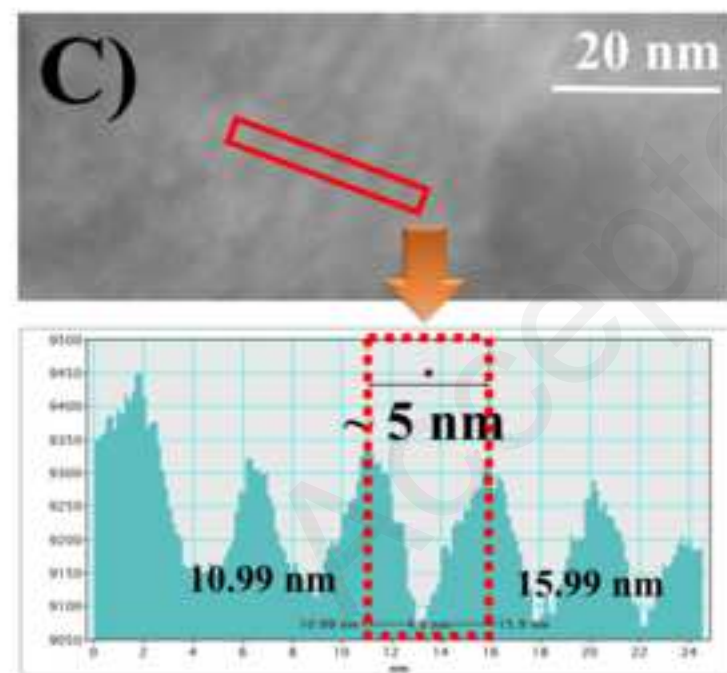
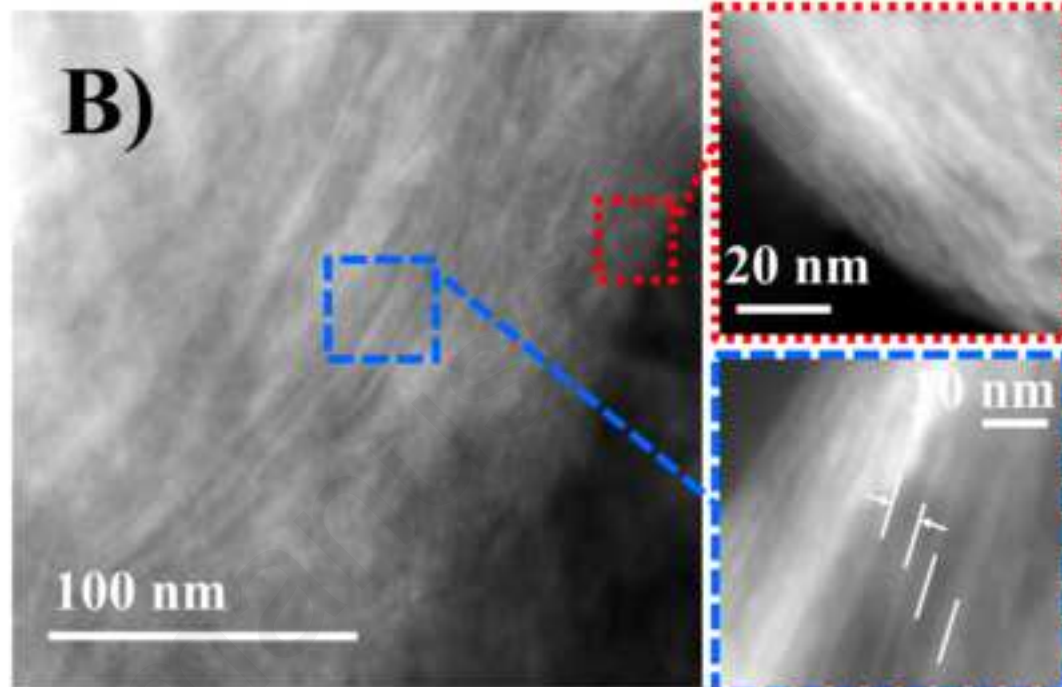
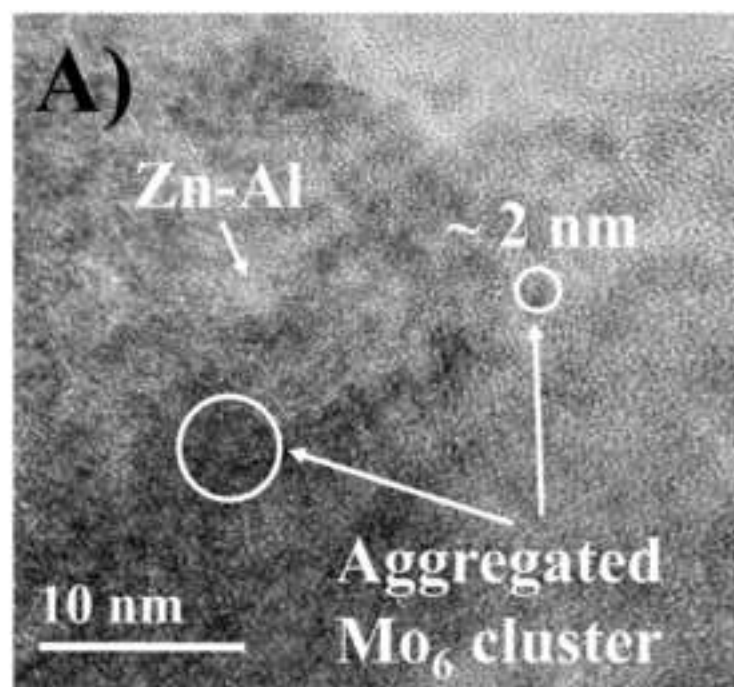


Figure
[Click here to download high resolution image](#)

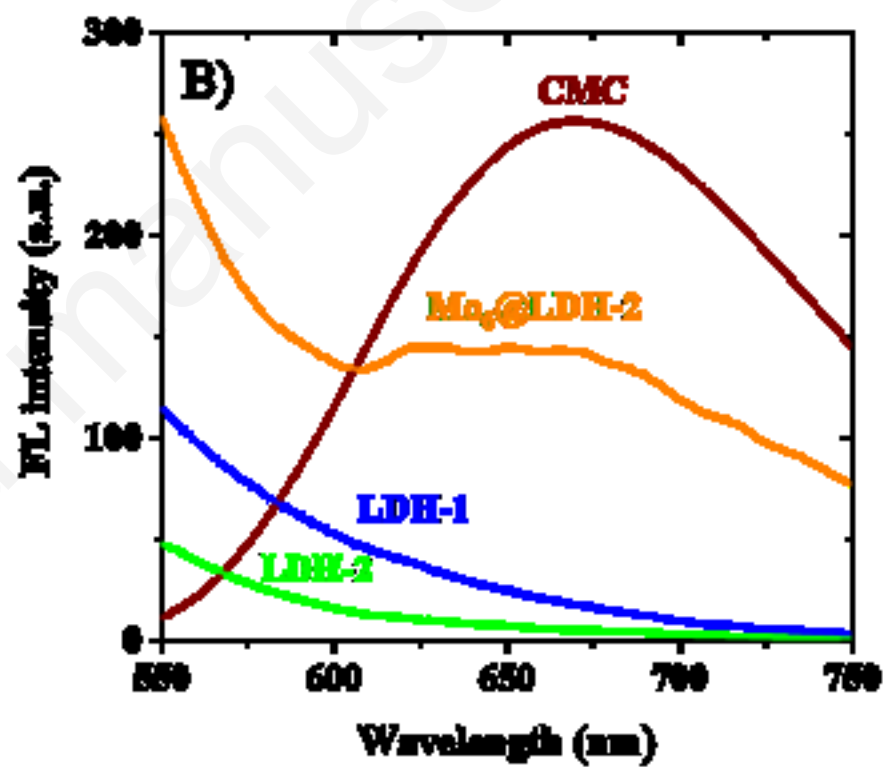
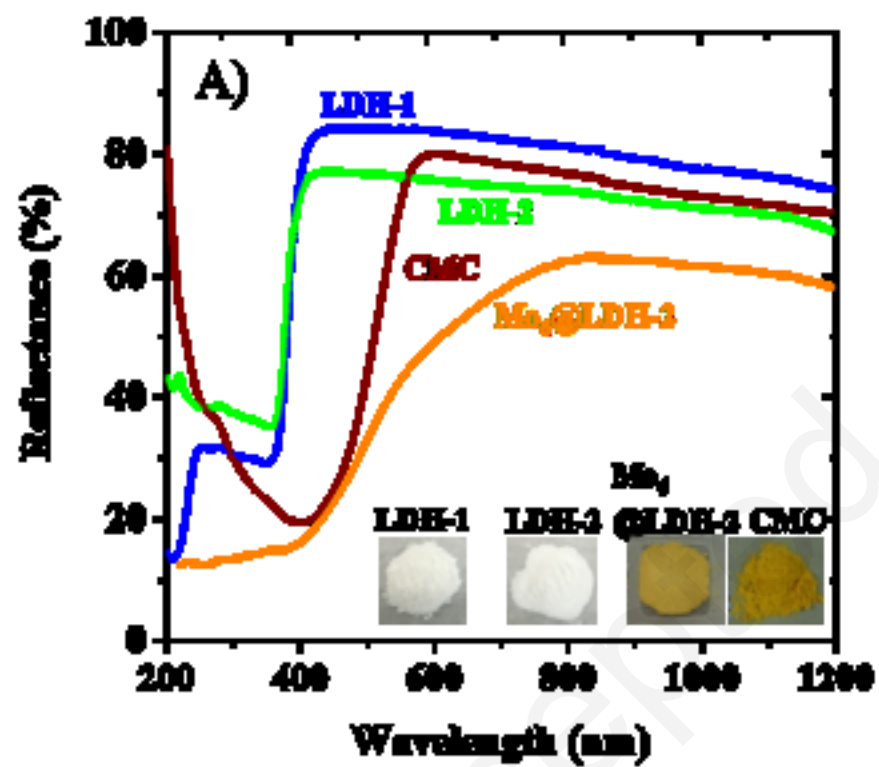


Figure
Click here to download high resolution image

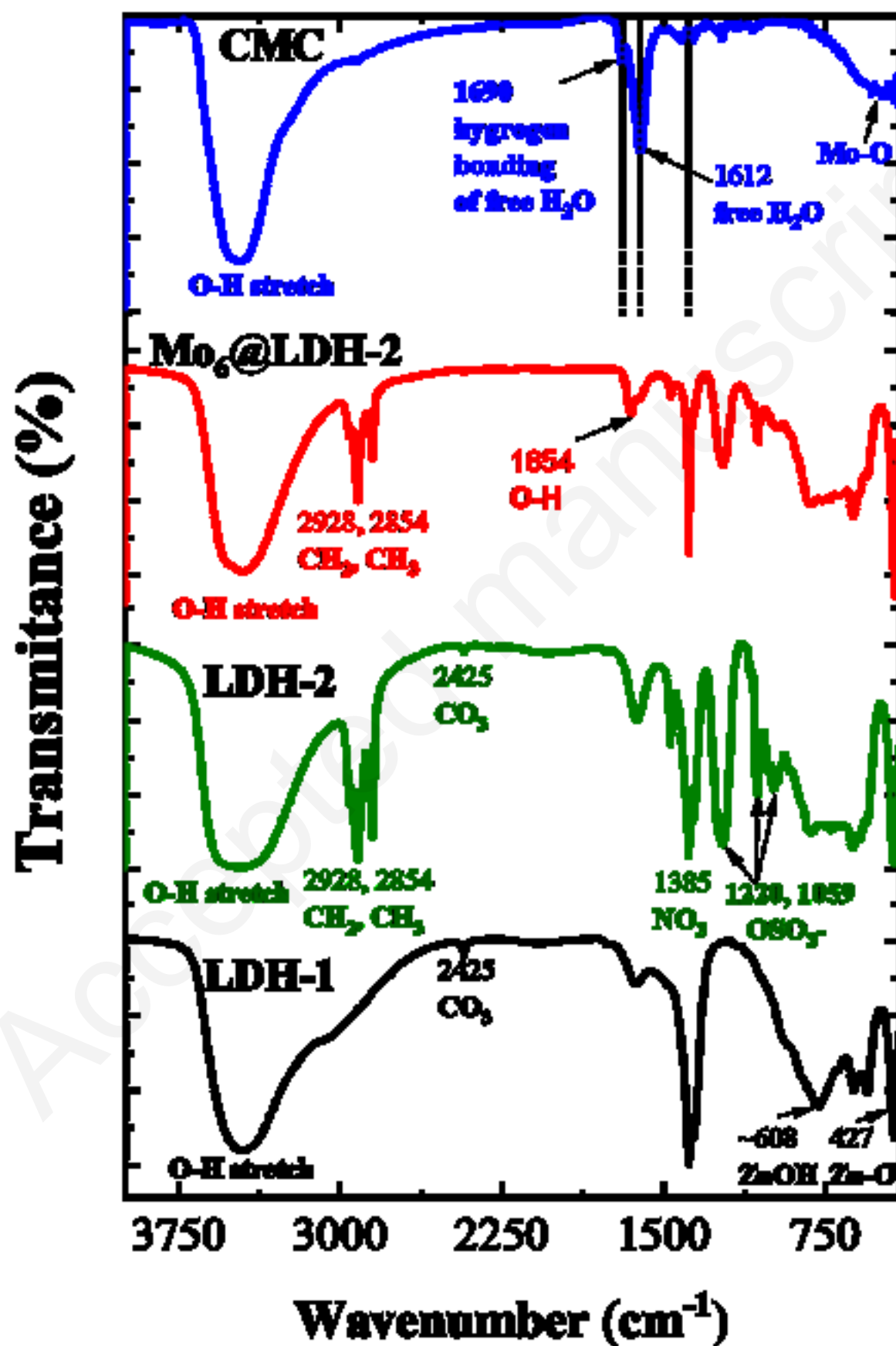
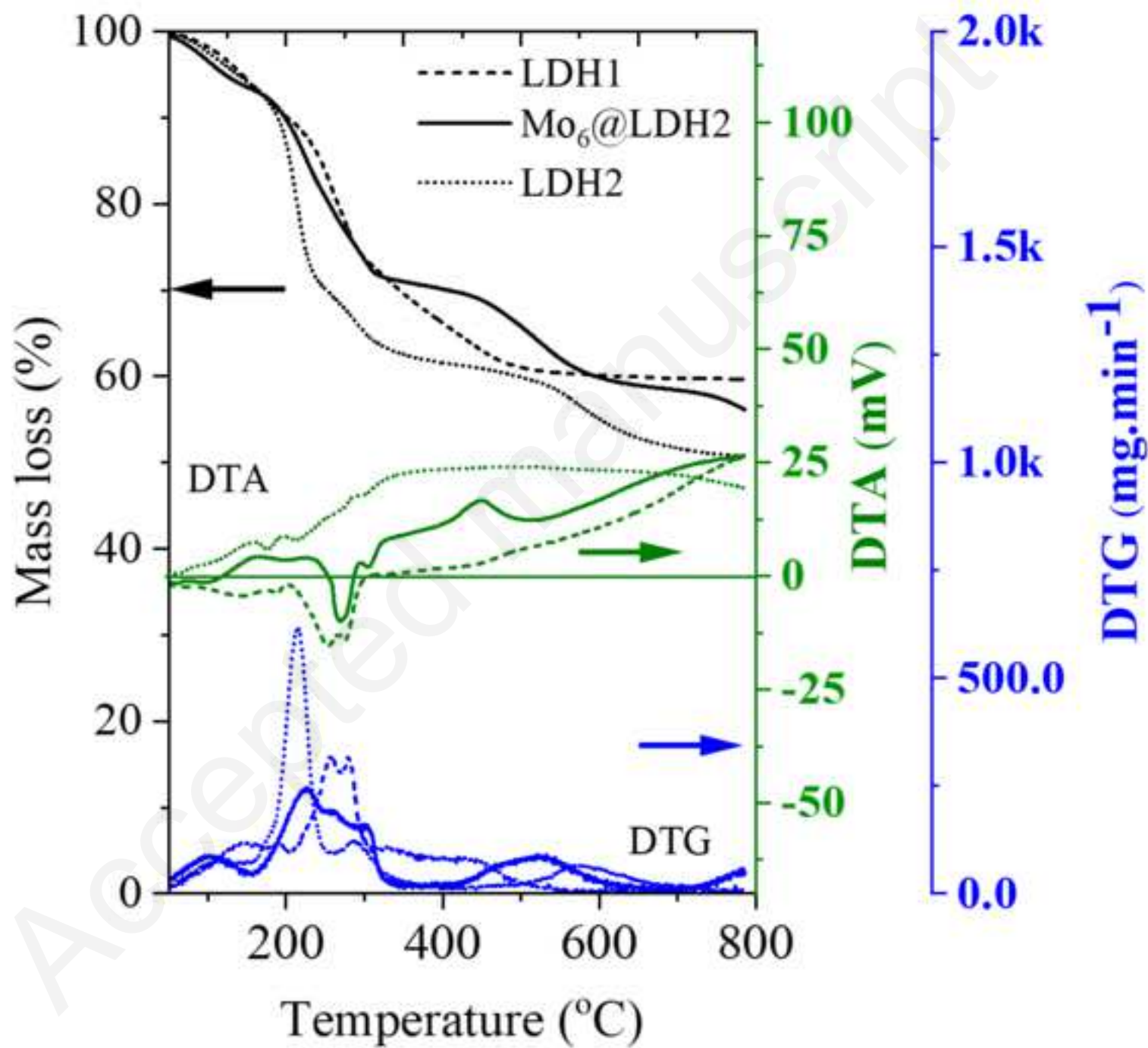
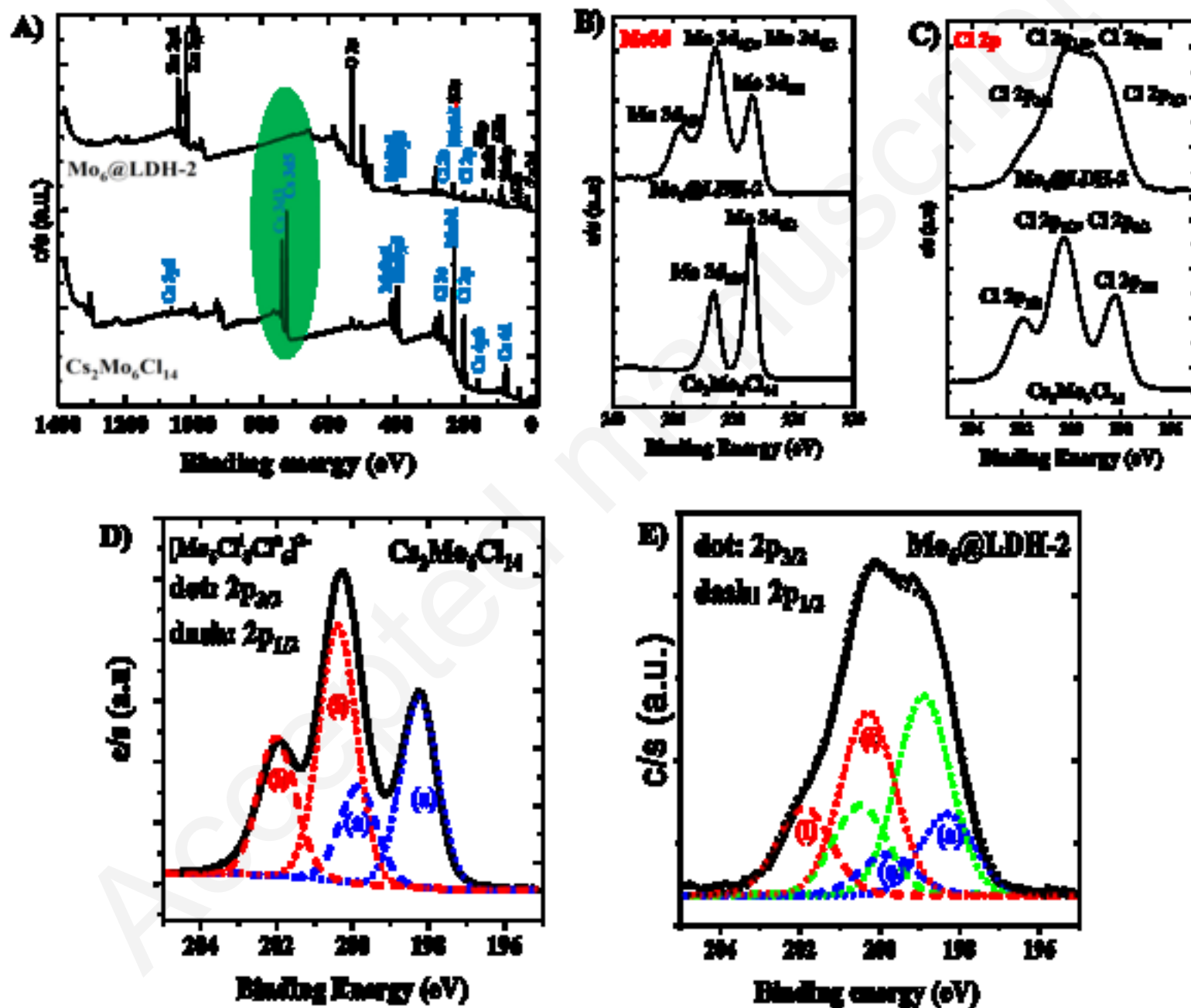


Figure
[Click here to download high resolution image](#)

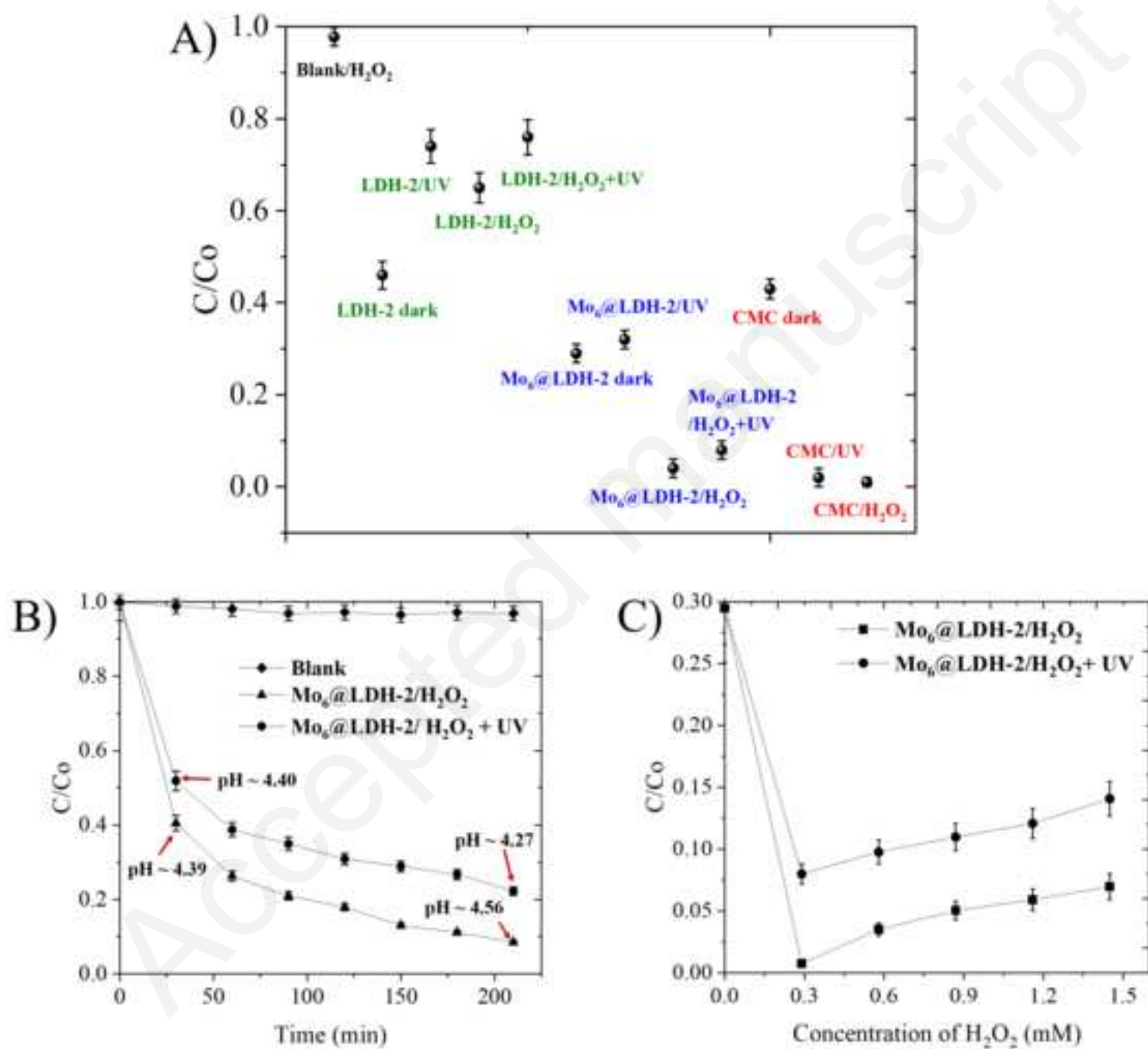


Figure

[Click here to download high resolution image](#)



Figure

[Click here to download high resolution image](#)

Figure

[Click here to download high resolution image](#)

